Effects of high magnetic fields on charge-density waves in $NbSe_3$

R. V. Coleman, M. P. Everson, Hao-An Lu, and A. Johnson
Department of Physics, University of Virginia, Charlottesville, Virginia 22901

L. M. Falicov
Department of Physics, University of California, Berkeley, Berkeley, California 94720
and Materials and Chemical Sciences Division, Lawrence Berkeley Laboratory, Berkeley, California 94720
(Received 24 April 1989)

The magnetotransport properties of $NbSe_3$ in the temperature range below the second charge-density-wave (CDW) onset of 59 K have been studied in magnetic fields up to 230 kG. At liquid-helium temperatures giant magnetoquantum oscillations caused by magnetic breakdown (MB) between the normal Fermi surface (FS) and open orbits on the nested sheets of the FS dominate the magnetotransport and are extremely sensitive to the pinned CDW configuration. Spatial variations in the phase of the pinned CDW change the local Fermi level and CDW gap, giving rise to a distribution of FS cross-sectional areas. These variations in FS cross section and CDW gap produce frequency shifts, amplitude modulations, and beat structures in the quantum oscillations observed in both the magnetoresistance and Hall effect. A model conductivity tensor has been developed describing the open-orbit network and MB interference as well as the closed-orbit contribution. The adjustable parameters of the model are the frequency of oscillation, the frequency-distribution spread ΔF, and critical MB parameter $\omega_0\tau$. The model has been used to study the detailed configurations of the pinned CDW in nominally pure $NbSe_3$ crystals and in $NbSe_3$ crystals doped with Fe, Ni, and Co. Unique fits to the data can be generated, and the resulting FS distributions provide direct information on the local CDW domain structure produced by pinning and repinning the CDW or by deliberately introducing impurities. At temperatures in the range 10–59 K, the oscillation amplitude decreases rapidly as the scattering time decreases, and a new magnetoresistance enhancement is observed. The dc resistance anomaly associated with the CDW is enhanced by up to a factor of 4 in a magnetic field of 226 kG and, if assigned exclusively to FS obliteration, it would require an increase from 60% obliteration at $H=0$ to 92% at $H=227$ kG. Accurate measurements also indicate a small increase in the transition temperature of ~ 0.5 K in a magnetic field of 226 kG. These results have been analyzed in terms of a theory proposed by Balseiro and Falicov in which a transverse magnetic field induces a more perfect nesting of the FS. Magnetic-field modifications of the electronic spectrum at the Fermi level can become large when the cyclotron energy $\hbar\omega_c$ is on the order of the CDW gap Δ. Both the enhancement of the magnetoresistance and the sign change in the Hall effect can be related to this mechanism. In addition to the magnetic-field-induced changes in the static CDW state, studies of the dynamics of CDW motion have also been carried out in magnetic fields up to 230 kG. The magnetoresistance response to the CDW motion can be modeled with equations similar to those of the Bardeen tunneling model. At high electric fields the enhanced magnetoresistance in the range 10–59 K is quenched; in the quantum-oscillation regime the enhanced dc magnetoresistance is quenched while the oscillation amplitude saturates. The large magnetoresistance in the static CDW state allows measurement of the threshold electric field down to low temperatures. For the nominally pure crystals the temperature dependence of E_T in high magnetic fields follows a thermal-fluctuation model similar to that observed at $H=0$, and the magnitude of E_T is not significantly changed from the values observed at $H=0$. At very low temperatures a departure from the dynamics of the tunneling model can give rise to a large region of zero dynamic resistance. This behavior is observed in the highest-purity crystals and is rapidly modified by impurities. The magnetic field facilitates the study of a large range of both static and dynamic CDW effects at low temperature: A systematic classification has been accomplished. Adequate theoretical models have been developed for several of the effects, although further refinement of the models and additional experimental confirmation are needed.

MS code no. BD4285 1990 PACS number(s): 71.25.Hc, 72.15.Gd

I. INTRODUCTION

We have studied magnetotransport phenomena in single crystals of $NbSe_3$ in the temperature range 1.2–59 K using magnetic fields up to 220 kG. Measurements have been made on crystals with residual resistance ratios ($\mathcal{R}$'s) in the range 10–285 covering the widest possible range of charge-density-wave (CDW) pinning phenomena. Niobium triselenide exhibits two independent CDW transitions,[1,2] one with an onset temperature $T_1=144$ K and the second with an onset temperature $T_2=59$ K.

Niobium triselenide is a quasi-one-dimensional metal

with a high conductivity along the chains of Nb atoms that run parallel to the **b** axis. The high-temperature Fermi surface (FS) is composed of nearly planar sheets oriented perpendicular to the **b** axis; they provide the nesting conditions which drive the CDW transitions. Band-structure calculations[3] suggest that the CDW transition at T_1 arises from FS sheets that produce nearly perfect nesting, while the transition at T_2 arises from only partially nested sheets. These transitions result in a substantial reduction of the FS area, but the remaining normal FS sections provide for semimetallic conductivity down to the lowest temperatures.

The low-temperature FS is therefore composed of electron and hole pockets remaining from the partially nested FS sections plus possible FS sections, formed from one high-temperature band that does not nest. The low-temperature FS topology is therefore fairly complex with the general form of small closed pockets separated from the nested FS sheets by CDW gaps.

The application of magnetic fields is observed to have unusually large effects on the low-temperature magnetotransport, and these effects constitute new and unusual mechanisms for electron transport in the presence of CDW's and magnetic fields. The major effects are observed below $T_2 = 59$ K and are not observed at high temperatures where only the one CDW exists with nearly perfect nesting. In this paper we concentrate on observations of magnetotransport in the temperature range 1.1–59 K.

At intermediate temperatures in the range 10–59 K the magnetoresistance shows an unusual enhancement with magnetic field.[4,5] A mechanism for this change has been proposed by Balseiro and Falicov[6] (BF) and we interpret the magnetoresistance data in terms of the BF mechanism. The Hall effect shows a reversal of sign as a function of magnetic field in the same temperature range, and unusual behavior as a function of CDW motion is also observed.[7,8] The Hall effect in general can show more subtle and complex behavior than the magnetoresistance and we discuss various possible contributions to the magnetic-field dependence, including the BF mechanism.

The existence of electron and hole pockets arising from imperfect nesting of the FS sheets, responsible for the CDW transition at 59 K, provides the FS topology necessary for the BF mechanism. This mechanism involves tunneling between the electron and hole pockets and is dependent on the ratio of the cyclotron energy $\hbar\omega_c$ to the pertinent gap Δ, rather than on $\omega_c\tau$ as in the usual magnetoresistance mechanisms.

At very low temperatures < 10 K, the magnetoresistance increases rapidly as the dependence of the magnetoresistance on $\omega_c\tau$ becomes dominant. Large-amplitude magnetoquantum oscillations dominate the magnetoresistance below 4.2 K in magnetic fields up to 220 kG. Although the frequency of these oscillations is determined by small pockets of normal electrons, the main mechanism contributing to the oscillation amplitude is magnetic breakdown (MB) to open orbits existing on the FS sheets that nest to form the CDW condensate. The normal-electron pockets are closely coupled to the pinned CDW structure through the MB process and this coupling is extremely sensitive to the pinned configuration of the CDW. Deformation of the CDW can shift the local Fermi level, which changes both the extremal FS area of the pocket and the MB gaps. Frequency shifts and amplitude modulations are observed which have been explained by Everson *et al.*[9] using a model developed by Sowa and Falicov[10] for treating dephasing effects in MB.

The Sowa-Falicov model is a one-dimensional model for calculating the oscillatory conductivity parallel to a single open orbit that is coupled to small lens-shaped closed orbits by MB. With this simplified model the calculated component of the oscillatory magnetoresistivity parallel to the open orbit provided a good simulation of the actual experimental ac magnetoresistance effects observed in $NbSe_3$. The actual experiments on $NbSe_3$ generally measure the component of resistivity perpendicular to the expected open-orbit direction and this component was not considered in the simplified model. The component perpendicular to the open orbit should oscillate in a similar manner, but would be shifted in phase by 90° and calculation of this component must consider the closed-orbit magnetoresistance as well as that of the open orbit.

We have modified the Sowa-Falicov conductivity tensor to include the closed-orbit contribution, and have calculated the resistivity perpendicular to the open-orbit direction in order to obtain a more accurate simulation of the actual experimental data for specimens exhibiting a range of impurity pinning. We summarize the results of the simulation for data on the nominally pure crystals of $NbSe_3$ and present similar comparisons for new data on crystals doped with Fe, Ni, and Co. The doped crystals show an enhanced deformation of the static CDW and the associated FS. The results also demonstrate the unusual structure introduced into the oscillatory magnetoresistance and Hall voltage by the CDW pinning and MB processes.

The magnetoresistance and Hall effect have been studied both at low electric fields, corresponding to the static pinned CDW state, and at high electric fields where the CDW is in motion and nonlinear behavior is observed. The magnetic-field effects that are observed in the static CDW state are demonstrated and interpreted first, and include the following experimental observations. (1) Enhancement of the transverse magnetoresistance in the range 10–59 K by magnetic-field-induced changes in the electronic structure not related to $\omega_c\tau$ but to the ratio $\hbar\omega_c/\Delta$. (2) The resistance maximum and the onset temperature T_2 associated with the low-temperature CDW are shifted by the applied magnetic field. (3) The Hall effect reverses sign as a function of magnetic field and the Hall angle approaches 90° at the low temperatures. (4) At helium temperature large-amplitude low-frequency oscillations dominate the transverse magnetoresistance and indicate the presence of MB. (5) The quantum-oscillation frequency is a sensitive function of CDW deformation and the particular pinned state of the CDW. (6) The frequency shifts occur in both the magnetoresistance and Hall-effect oscillations and suggest the presence of a spatial distribution of FS areas. (7) Amplitude modulation, hysteresis and interference effects all confirm the ex-

istence of a spatial variation of FS areas and its consequent influence on the MB process.

These observations and processes apply to the magnetotransport phenomena observed when the CDW is static, at relatively low electric fields. At higher electric fields the CDW's can undergo motion[11,12] above certain threshold electric fields E_T, which are determined by the impurity pinning[13] of the CDW's. The large magnetoresistance makes it possible to apply larger dc electric fields at low temperatures than would be possible at $H=0$. At temperatures below 4.2 K this has led to the observation of large regions of high-conductivity CDW motion where dV/dI is zero over a range of currents in some high-purity specimens. This nondissipative flow of the CDW electrons exists only at low temperatures and becomes dissipative above 10 K, where thermal-fluctuation processes become dominant. We have also studied the effects of magnetic fields on the threshold electric fields and on the dynamics of CDW motion.

The nonlinear magnetoresistance observed for electric fields above threshold can be fitted to expressions similar to those used in the $H=0$ case. In the higher temperature range of 10–59 K either the Bardeen[14] tunneling-model expression or the semiclassical expression of Sneddon *et al.*[15] can be used to fit the magnetoresistance data in the nonlinear regime above threshold. However, at helium temperatures where the quantum-oscillatory component arising from the MB process is important, the analysis is more difficult. Similar phenomenological expressions can be used to fit the data quite well, but the components arising from the oscillatory MB and the nonlinear CDW motion couple so that no simple explanation is possible. We analyze and discuss the following experimental results of measurements on magnetotransport in the nonlinear regime. (1) The CDW magnetoresistance anomaly below 59 K is rapidly quenched by CDW motion, a result similar to the observation at $H=0$. (2) The oscillatory component of the magnetoresistance maintains a constant voltage amplitude over a large range of current above threshold at 1.1 K, where MB processes dominate. (3) The dc Hall voltage reverses sign as a function of magnetic field and this zero crossing moves rapidly to higher magnetic fields as the current and electric field increase above threshold at a given temperature in the range 10–59 K. (4) At helium temperatures the large transverse Hall voltage is a linear function of magnetic field. For some cases the Hall resistance remains ohmic above threshold, while the magnetoresistance becomes highly nonlinear. In other cases the Hall resistance also becomes nonlinear above threshold. (5) The threshold electric fields E_T in the nominally pure specimens show very little dependence on magnetic field. (6) The temperature dependence of E_T follows a thermal-fluctuation, exponential behavior in the nominally pure specimens, but this is strongly modified by Fe impurities.

The measurements of magnetotransport properties reported here represent a wide range of unusual electronic behavior introduced by the presence of CDW's in a highly anisotropic metal. They demonstrate the extraordinary complexity of electronic structure and FS effects encountered in $NbSe_3$, but at the same time show that a systematic analysis is possible for most of the effects. Although some details require further work, the data and analysis provide a fairly complete picture of the magnetotransport mechanisms operating in $NbSe_3$. However, more experiment and analysis are required to confirm the microscopic models and to develop a more complete picture of the FS topology, as affected by both the static and dynamic CDW structure.

II. EXPERIMENTAL TECHNIQUES

The $NbSe_3$ and doped $NbSe_3$ crystals were grown by vapor transport in sealed evacuated quartz tubes using mixed powders of the starting elements. They were first sintered at 800–1000 °C to give a free flowing metallic powder of appropriate composition. The crystals were then grown for one to two weeks at a temperature of ~750 °C in a temperature gradient of approximately 10 °C/cm.

In the case of the pure crystals Nb powder of 99.99% purity and Se powder of 99.999% purity was sintered to produce the starting powder. The nominally pure crystals gave $\mathcal{R}$ ($R_{300\,K}/R_{4.2\,K}$) in the range 50–280. The largest quantum-oscillation amplitudes were obtained on crystals with $\mathcal{R} \geq 200$.

Studies have also been carried out on crystals deliberately doped with Fe, Ni, and Co in the composition M_xNbSe_3, where x is in the range 0.01–0.05. At these concentrations the Fe, Ni, or Co impurities do not enter the Nb chains and the quantum-oscillation amplitude remains quite large even though the $\mathcal{R}$'s are reduced to the range 20–50. The pinning of the CDW is also increased substantially, as detected by the frequency spread of the quantum oscillations. The concentration of Fe in the crystals of the form Fe_xNbSe_3 has been checked by chemical and secondary ion emission analysis, and the results show that the crystals incorporate an order of magnitude less Fe than that added to the starting powder. Further details of the secondary ion emission results on the Fe doping are given in Sec. III A 3. The Ni and Co doping concentrations have not been checked in detail, but the transport properties and CDW pinning show similar features to those observed for Fe_xNbSe_3, indicating a limited incorporation of the Ni or Co atoms into the growing crystal.

The quantum-oscillation shifts that are described in this paper are observed for all ranges of $\mathcal{R}$'s tested. The frequency spread and degree of shift becomes progressively larger as $\mathcal{R}$ decreases and the impurity concentration increases, but pinning of the CDW by impurities modifies the normal FS in all cases.

The crystals were mounted on printed circuit blocks with copper pads and silver paint. The magnetoresistance measurements were made using a four-terminal contact configuration with a counter emf loop printed on the circuit block. The Hall voltage was measured with a single pair of contacts on opposite faces of the crystal. The correction for any magnetoresistance component was very small because of the large magnitude of the Hall voltage. Fine copper leads, noninductively wound, were used to make all the connections from the circuit block to

the top of the Dewar, where conventional shielded cable connections were made.

The mounted crystal and circuit block were glued to a gear-driven rotator immersed in a bath of liquid helium and pumped to a temperature of ~1.2 K. A superconducting solenoid was used for magnetic fields in the range 0–70 kG and the Bitter solenoids at the Francis Bitter National Magnet Laboratory were used for the range 0–230 kG. The dc magnetoresistance and Hall voltage were recorded with a conventional microvoltmeter driving an *XY* recorder and a computer. The oscillatory components of the magnetoresistance and Hall voltage were also recorded using ac techniques. Harmonic detection was used with a lockin amplifier and modulation of the magnetic field at frequencies in the range 7.5–15 Hz. A modulation coil was mounted in the bore of the superconducting solenoid; the Bitter solenoids were modulated directly by modulating the generators at 7.5 Hz. The data were recorded with an on-line computer and the Fourier transforms were generated directly from the computerized data. The data were usually recorded in the second harmonic mode.

III. EXPERIMENTAL RESULTS

The experimental results are divided into two main sections covering (a) the magnetotransport effects observed when the CDW is static, and (b) when it is in motion producing a nonlinear response of the transport coefficients. With these categories we consider two separate temperature ranges where different fundamental mechanisms dominate the magnetotransport. These are the very-low-temperature range of 1.1–4.2 K, where quantum-oscillatory effects related to MB play the primary role and a higher-temperature range from 10 to 60 K, where direct modifications of the energy spectrum at the Fermi surface by the magnetic field produce unusually large changes in the transport coefficients as a function of magnetic field. The CDW structure plays a crucial role in all these regimes, and we systematically describe the many experiments and results starting with the static CDW regime first.

A. Magnetotransport in the pinned CDW state

These experiments were carried out at low electric fields, where the electric field remained well below threshold for the entire range of applied magnetic fields. The initial magnetic-field response was usually measured after cooling from room temperature and applying electric fields that remain below threshold. Subsequent data were then obtained for new states of the pinned CDW induced by applying large electric fields, depinning the CDW, and then repinning it by reducing the electric field below threshold. The magnetic-field response was then again measured and compared to the initial state. Changes in response due to changes in magnetic and electric-field direction were also measured.

1. Large-amplitude low-frequency quantum oscillations in magnetoresistance

As previously reported in a number of studies[9] the magnetoquantum oscillations at low temperature are dominated by a few low frequencies representing extremal orbits on the FS, with cross-sectional areas representing $\sim 10^{-3}$ of the Brillouin zone (BZ) cross section. For the magnetic field parallel to the **c** axis and current parallel to the **b** axis one single frequency of ~0.3 MG is usually observed. This frequency increases[9,16,17] smoothly as the magnetic field is rotated in the **a**-**c** plane, reaching a maximum of ~1.0 MG at **H**⊥**c**. Recent experiments[9] have also shown that this frequency could be shifted in a range from ~0.28 to ~0.32 MG for **H**∥**c** by creating various metastable states of the pinned CDW. A similar behavior is observed for most directions of **H** in the **a**-**c** plane. This can occur spontaneously, or in a controlled way by depinning and repinning the CDW through brief application of an electric field above the threshold for CDW motion.

Figure 1 shows an example of a dc magnetoresistance curve recorded for a field range of 0–230 kG. The lower curve was the initial response before depinning. The upper curves were obtained after depinning and repinning the CDW in a new configuration. The frequency has shifted to a lower value and the background magnetoresistance has increased. This is a *bona fide* frequency shift, and not a phase shift. The frequency is also definitely lower and both of these points are confirmed in the ac magnetoresistance data presented later. One additional point with respect to the dc curve in Fig. 1 is that 80% of the total magnetoresistance change is in the oscillating component. This is strong evidence that enhancement by MB is occurring rather than simple modulation

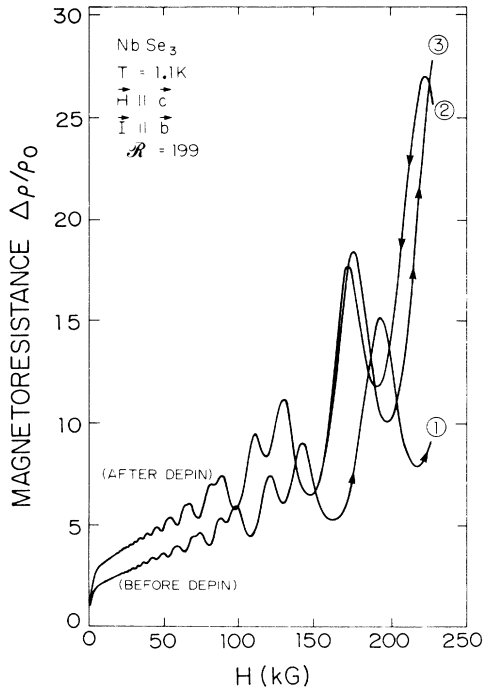

FIG. 1. Quantum oscillations observed in the dc transverse magnetoresistance of $NbSe_3$ before and after depinning the CDW at 1.1 K. A frequency shift from 0.31 to 0.28 MG is induced by depinning and repinning the CDW; **I**∥**b** and **H**∥**c** (from Ref. 5).

of the density of states at the FS, as in the ordinary Shubnikov–de Haas effect.

For some quite pure $NbSe_3$ crystals it is possible to shift the frequency by reversing either the electric field or the magnetic field without depinning the CDW. This is a reversible process and is demonstrated in the ac magnetoresistance data of Fig. 2. Figure 2(a) shows the oscillatory magnetoresistance for $\pm I$ and $+H$, and Fig. 2(b) shows it for $\pm H$ and $+I$. The frequency shift is identical for both experiments, and moves from 0.28 to 0.31 MG, as is clearly resolved in the Fourier transforms of Fig. 3. The solid and dashed lines match the data of Fig. 2. The Fourier transforms also show a large harmonic content partially caused by the spin splitting, but also consistent with the MB process to be discussed in Sec. IV.

The experiment just described shows that the sign of $(\mathbf{H}\times\mathbf{I})$ is the important factor, and this checks out for the additional two combinations of I and H not shown. This result suggests that the transverse Hall electric field, which can be much larger than the longitudinal electric field, is the critical factor which shifts the static CDW configuration in this case.

The frequency shift is typical of the whole range of $\mathcal{R}$'s studied and, although the stability and conditions required to shift the frequency are variable, the general relation of the frequency to specific metastable CDW states is observed for a wide range of crystals. Similar effects are observed for the crystals doped with Fe, Ni, and Co discussed in Sec. III A 3.

2. *Beat structure and MB interference in the magnetoresistance of $NbSe_3$*

In addition to the frequency shifts described earlier many of the as-cooled crystals show an unusual beat structure, as shown in the example of Fig. 4. Figure 4(a) shows a clear beat at ~25 kG in a magnetic-field sweep from 0 to 70 kG, and the Fourier transform of Fig. 4(b) shows the expected frequency splitting consistent with

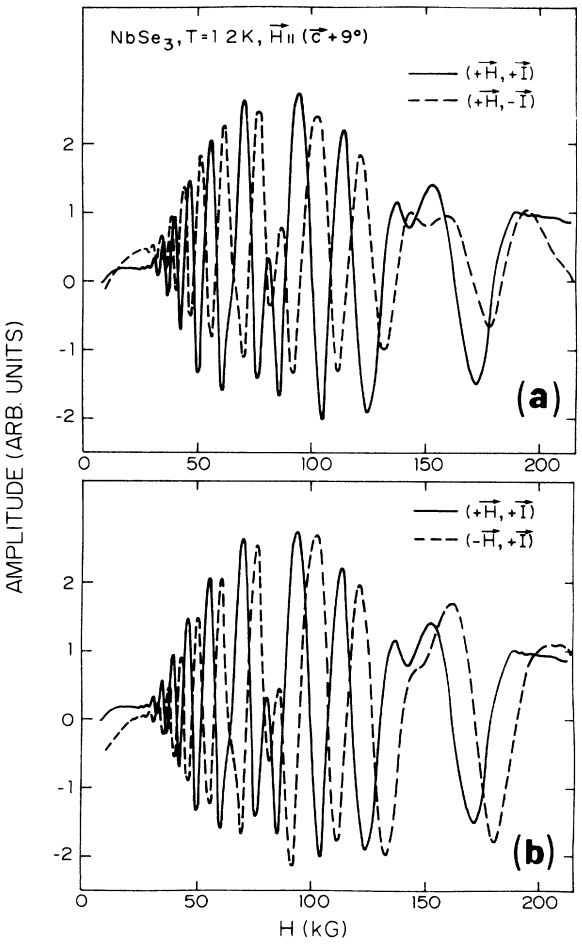

FIG. 2. Frequency shifts observed in the ac transverse magnetoresistance of $NbSe_3$ when the current or magnetic field are reversed at 1.1 K. In this case the electric field remains below the threshold electric field E_T. (a) $(+\mathbf{H}+\mathbf{I})$ and $(+\mathbf{H},-\mathbf{I})$, (b) $(+\mathbf{H},+\mathbf{I})$ and $(-\mathbf{H},+\mathbf{I})$.

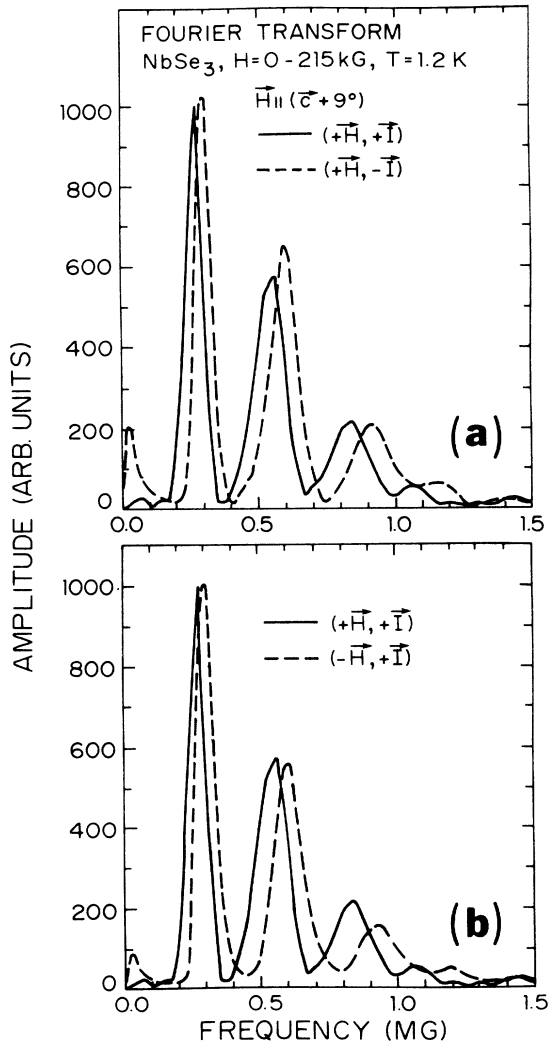

FIG. 3. Fourier transforms of the ac magnetoresistance data shown in Fig. 2. A reversible frequency shift of ±0.03 MG is observed for reversal of either **H** or **I**. The maximum frequency is 0.31 MG and the minimum frequency is 0.28 MG; (a) $(+\mathbf{H},+\mathbf{I})$, and $(+\mathbf{H}-\mathbf{I})$; (b) $(+\mathbf{H}+\mathbf{I})$ and $(-\mathbf{H}+\mathbf{I})$.

the beat. The frequencies are 0.35 and 0.38 MG. This beat is not caused by two distinct FS cross sections, but results from a single piece of the FS that interacts with the CDW to give a distribution of extremal areas. The beat is produced by interference effects generated through MB. Details of the MB model are given in Sec. IV.

The beat structure is observed for a large range of magnetic-field directions in the **a-c** plane, and Fig. 5(a) shows a similar beat observed at a magnetic-field angle 60° from the **c** axis, while Fig. 5(b) shows the oscillatory magnetoresistance generated by a computer calculation of the MB model, with a spread of FS areas giving a beat corresponding to frequencies of 0.39 and 0.41 MG. The model neglects the spin splitting and we have calculated the first derivative rather than the second derivative because of numerical noise considerations. Therefore the amplitudes generated by the model are not accurate at higher magnetic fields, but the determination of the frequency spread and the observed beat structure is very accurate.

The crystal used for the data of Fig. 5 was a nominally pure crystal with a high $\mathcal{R}$ of 284; the data are shown for a magnetic-field range of 0–70 kG. Some crystals show an even greater frequency spread, and a strong beat structure at higher magnetic fields can be resolved. An example is shown in Fig. 6(a) for a magnetic-field sweep of 0–220 kG. Additional beats are present at lower fields but the large magnetic-field modulation of ~2 kG washes these out. Figure 6(b) shows the curve generated by the MB model, which requires a frequency interval of 0.31–0.36 MG.

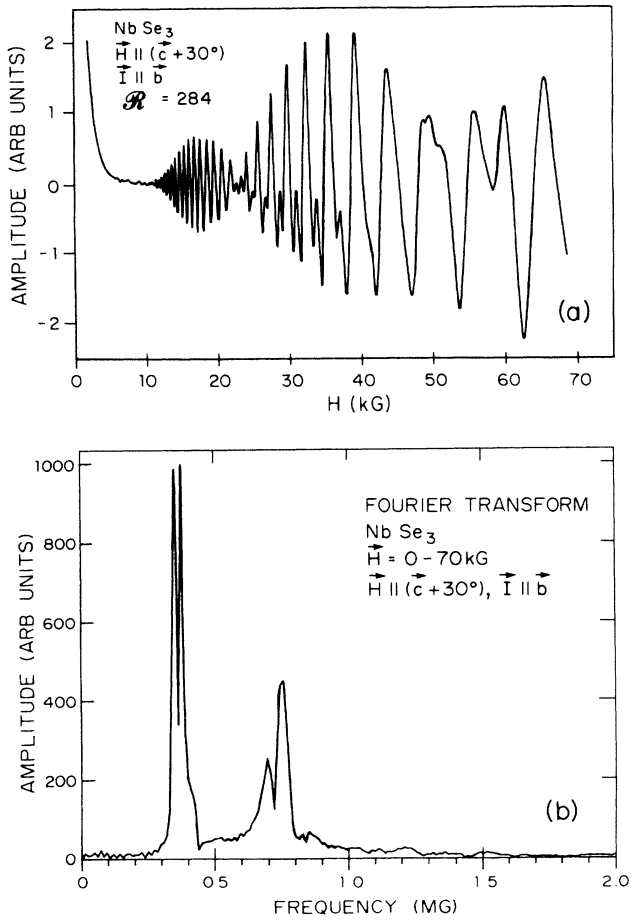

FIG. 4. (a) ac transverse magnetoresistance in $NbSe_3$ observed from 0 to 70 kG using $2f$ harmonic detection at 1.1 K. Data were recorded using a pure as-cooled crystal with $\mathcal{R}=284$ and $\mathbf{H}\|(\mathbf{c}+30°)$. The beat structure was observed over a range of magnetic-field orientations. (b) Fourier transform of the data showing frequency split of 0.35–0.38 MG resulting from the beat structure (from Ref. 9).

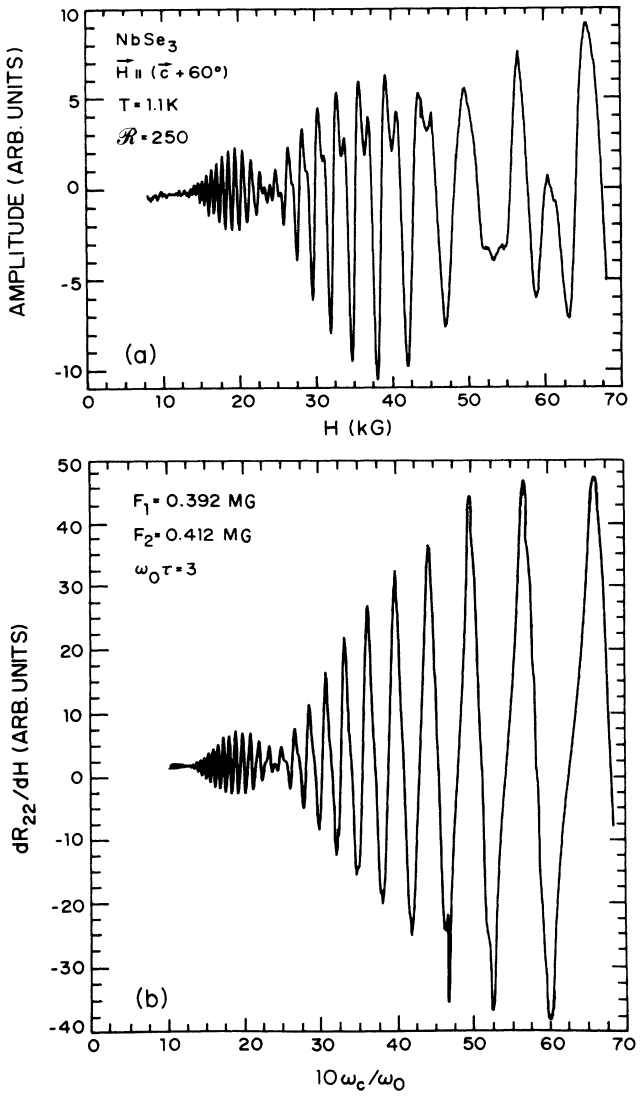

FIG. 5. (a) ac transverse magnetoresistance at 1.1 K in a pure $NbSe_3$ crystal with $\mathcal{R}=250$ showing beat structure for $\mathbf{H}\|(\mathbf{c}+60°)$. (b) Model calculation based on the MB network described in Sec. IV. A frequency spread from 0.392 to 0.412 MG is required to generate the observed beat; ω_c is the cyclotron frequency and ω_0 is the critical MB frequency. The ratio scale matches the experimental scale measured in kG.

In the preceding experiments on nominally pure crystals, depinning of the CDW by applying a brief electric field above threshold generally removes the beat structure and produces a single frequency at the low end of the frequency spread observed before depinning. This frequency shift to a single lower frequency can also be observed in the doped crystals, as demonstrated for Ni_xNbSe_3 in the next section. However, the doped crystals can also show a redistribution of FS areas after depinning and repinning that generates a substantial frequency interval and spread of FS areas. As the pinning becomes greater, the spread in the FS areas becomes larger, and a spectrum of metastable states can be observed after repinning. Examples are shown for Co_xNbSe_3 later.

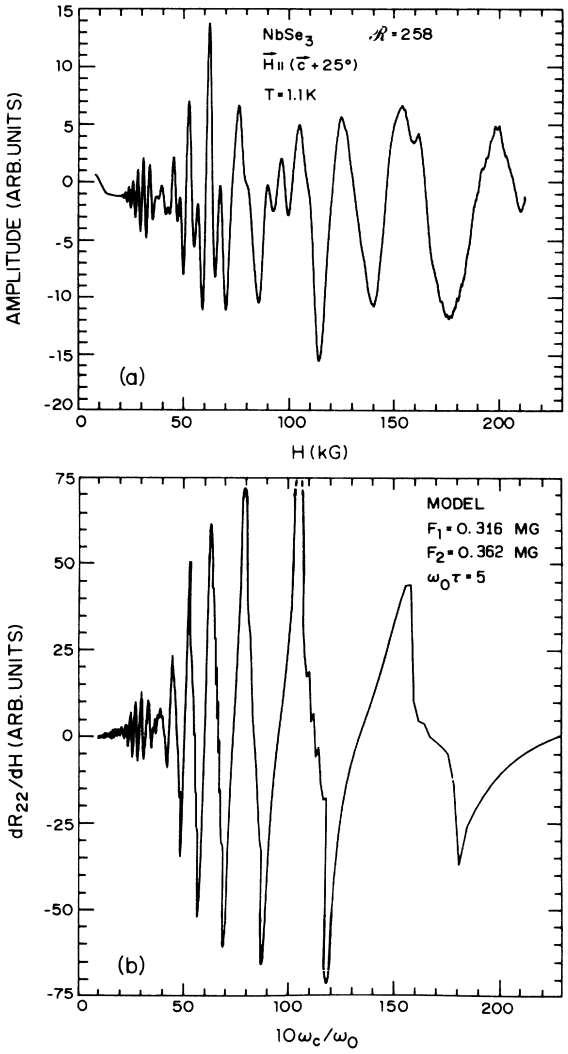

FIG. 6. (a) ac transverse magnetoresistance for the field range 0–210 kG. The beat at ~35 kG indicates the existence of a very large frequency spread in the as-cooled state. The data were recorded for a pure crystal ($\mathcal{R}=258$) at 1.1 K with $\mathbf{H}\|(c+25°)$. (b) The model calculation that fits the beat structure requires a frequency spread from 0.316 to 0.362 MG.

3. *Beat structure and MB interference in the magnetoresistance of Ni_xNbSe_3, Fe_xNbSe_3, and Co_xNbSe_3*

In order to increase the impurity pinning we have doped the starting growth powder with Ni, Fe, and Co. These impurities decrease the $\mathcal{R}$ and increase the CDW pinning, but do not destroy the amplitude of the quantum oscillations. At starting concentrations of $x=0.01-0.05$ they do not disrupt the Nb chain structure, and T_2 for the CDW onset is depressed only slightly. Spectroscopic analysis of the Fe doping shows that the final concentration in the crystal is reduced by 2 orders of magnitude from that of the starting powder. Secondary ion emission studies also show that the concentration is approximately uniform from the surface to a depth of at least ~500 Å as indicated in the data of Fig. 7.

Doping with Ni reduces the $\mathcal{R}$ of the crystals to typical values in the range 20–50. At the same time the beat structure is more pronounced after the initial cooldown, while the threshold E_T for CDW motion at 1.1 K is only increased by a factor of 2 from the values measured for the nominally pure crystals at 1.1 K. Figure 8(a) shows ac magnetoresistance data for a $Ni_{0.03}NbSe_3$ crystal in the magnetic-field range 0–70 kG. A prominent beat structure is observed and the model fit to the data, as shown in Fig. 8(b), requires a frequency spread from 0.28 to 0.32 MG, a spread substantially larger than usually observed in the nominally pure crystals. This frequency spread is

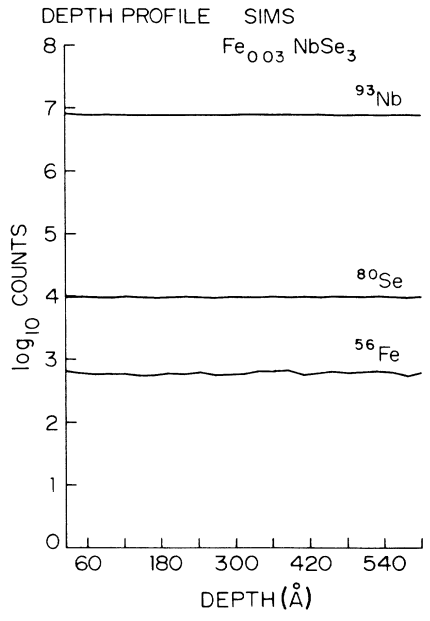

FIG. 7. Depth profiles obtained from secondary ion mass spectrometry of a crystal grown from a starting powder of composition $Fe_{0.03}NbSe_3$. The final concentration of Fe in the crystal was 2 orders of magnitude less than in the starting powder, as estimated from calibration standards. The dilute Fe concentration was, however, uniformly distributed within a given depth profile, but could vary by a factor of 2 for different areas of the crystal or for different crystals from the same batch.

confirmed in the Fourier transform of the direct data, as shown in Fig. 9(a). In addition, both the direct ac data and the second harmonic amplitude in the Fourier transform show that the Ni has quenched the spin splitting in this magnetic-field range. After briefly depinning the CDW at high electric fields, the repinned CDW structure no longer induces a beat structure in the ac magnetoresistance and the Fourier transform shows a single frequency at 0.28 MG, as shown in Fig. 9(b). The disappearance of the beat structure after depinning and repinning the CDW is a general phenomenon observed for most of the nominally pure crystals as well as the lightly doped crystals. The CDW motion at low temperature appears to reduce substantially the spread in FS cross sections as well as to reduce the average FS cross section throughout the crystal. The beat structure can be recovered by warming the crystal above the CDW transitions and requenching it to helium temperatures. In some cases depinning and repinning of the CDW at 1.1 K modifies the beat structure, but does not eliminate it. Preliminary evidence suggests that this occurs in the more heavily doped crystals, where a wider frequency distribution is observed and a more complex beat structure is often present. Examples observed for Fe and Co doping are presented later.

Figure 10 shows three ac magnetoresistance field sweeps in Fe_xNbSe_3 corresponding to CDW states obtained in a first cooldown from room temperature, a second cooldown from room temperature, and a depinning and repinning of the CDW at 1.1 K. As shown in Fig. 10(a) a single-beat structure, very similar to that observed in the previous examples, is present after the first cooldown. After the second cooldown a more complex two-beat structure is observed, as shown in Fig. 10(b). After depinning at 1.1 K in a strong electric field the complex beat structure is entirely eliminated, as shown in Fig. 10(c). The Fourier transforms of the Fe_xNbSe_3 data

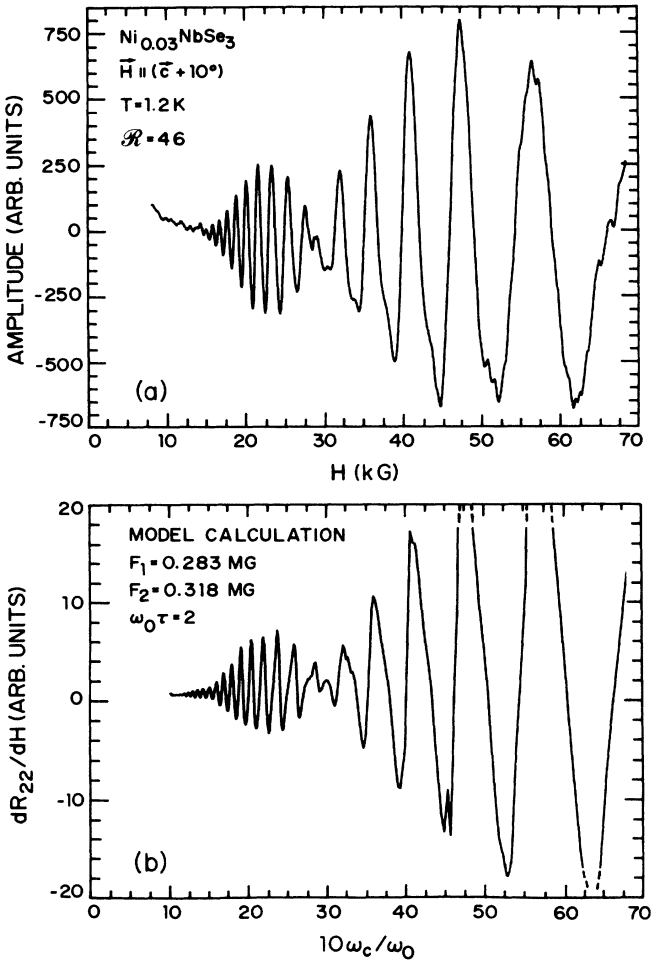

FIG. 8. (a) ac transverse magnetoresistance measured in a Ni-doped single crystals of $NbSe_3$ grown from a starting powder of composition $Ni_{0.03}NbSe_3$. The field range was 0–70 kG with a beat minimum at 30 kG and fewer oscillations within the beat period than generally observed in the as-cooled pure crystals at the same field orientation of $\mathbf{H}\|(c+10°)$. This indicates a fairly large frequency spread as confirmed in the model calculation shown in Fig. 8(b). (b) Model calculation of the transverse magnetoresistance generating the correct beat structure using a frequency spread from 0.283 to 0.318 MG.

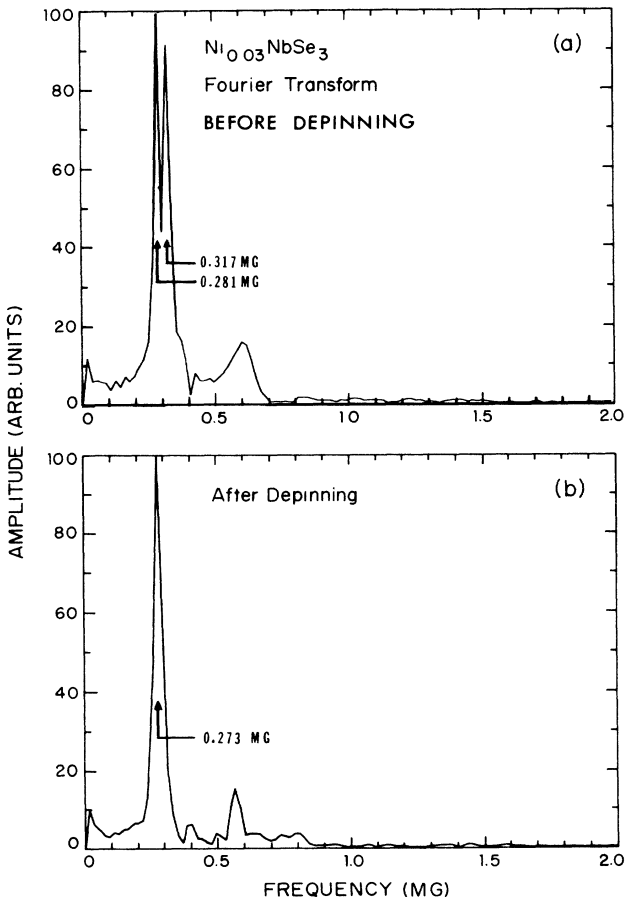

FIG. 9. (a) Fourier transform of data on the Ni-doped $NbSe_3$ crystal shown in Fig. 8(a). The frequency splitting corresponds to minimum and maximum frequencies of 0.30 and 0.33 MG, respectively, in good agreement with the model calculation of Fig. 8(b). (b) Fourier transform of ac magnetoresistance measured after depinning the CDW at 1.2 K. A single low frequency of 0.27 MG is present.

in Fig. 10 are shown in Fig. 11. The frequency spreads observed after each of the cooldowns are 0.28–0.32 MG and 0.28–0.34 MG, respectively. After depinning the CDW in a strong electric field at 1.1 K a single sharp frequency of 0.28 MG is observed in the repinned static CDW state. The data of Fig. 10 on Fe_xNbSe_3 can also be fitted quite well with the MB model. However, the required distribution of frequencies in the metastable CDW states can be more complex than required for the nominally pure crystals. Details of the MB model calculation are given in Sec. IV.

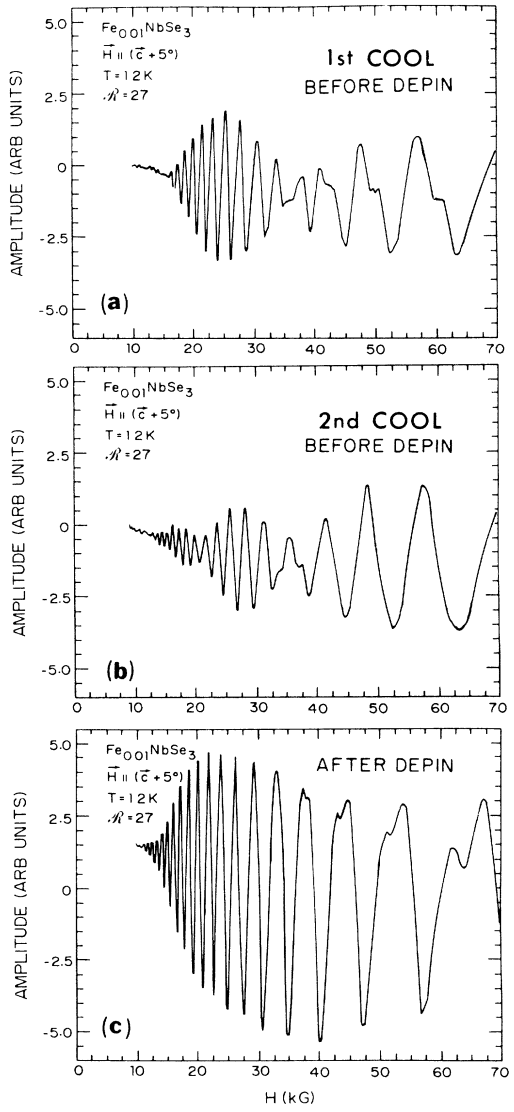

FIG. 10. ac transverse magnetoresistance observed in an Fe-doped $NbSe_3$ crystal grown from a powder of starting composition $Fe_{0.03}NbSe_3$. The $\mathcal{R}=27$ with $\mathbf{H}\|(c+5°)$ (Ref. 3) and the field range was 0–70 kG. (a) Data recorded after first cooldown and no depinning of the CDW. A single beat is present. (b) Data recorded after second cooldown and no depinning of the CDW. A more complex double beat is observed. (c) CDW has been depinned and repinned at 1.2 K. The beat structure has been removed and a single frequency of larger amplitude is observed.

In addition to the collapse of the frequency spread, the amplitude of the oscillation significantly increases after the CDW depinning has created a CDW state of more uniform FS cross-sectional areas. This amplitude increase was also observed in the dc data when the frequency was shifted by CDW depinning. The direct connection between the amplitude increase and the elimination of beats suggests that the MB interference becomes more coherent in the uniform state, introducing a greater modulation by the MB interference phenomena in the orbit network.

For Co_xNbSe_3 crystals a similar behavior is observed, and an example is shown in Fig. 12, where the beat struc-

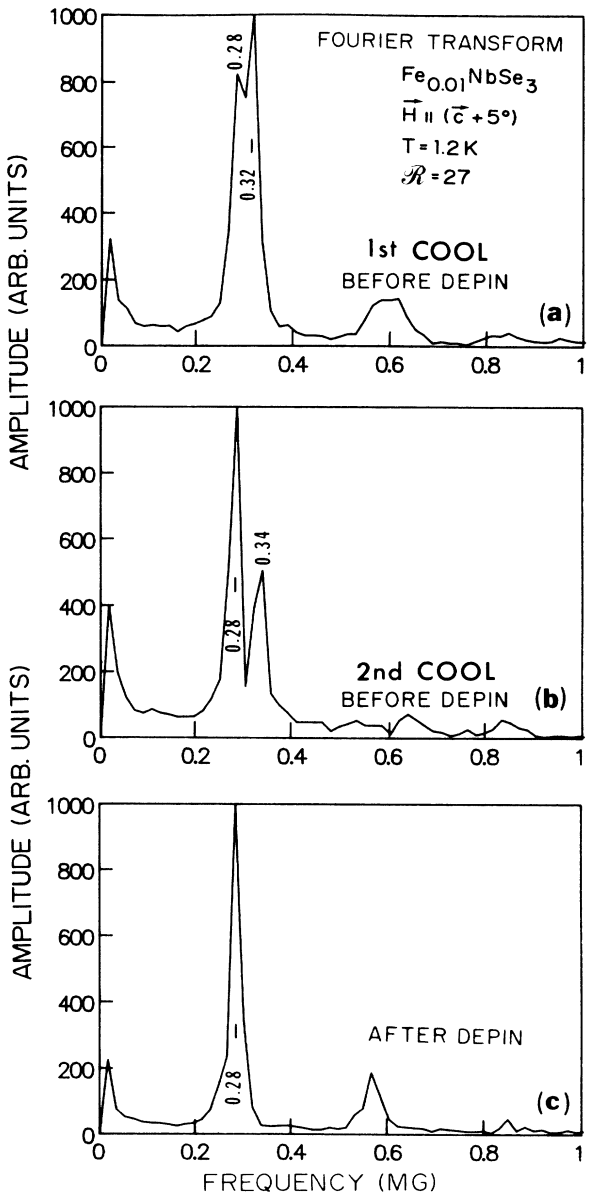

FIG. 11. Fourier transforms of the experimental magnetoresistance data shown in Fig. 10. Frequency at each peak is listed in MG. The frequency splittings should be compared with the frequency distributions generated by the model calculations which are shown in Fig. 38.

ture can be changed by depinning and repinning the CDW at 1.1 K. Figure 12(a) shows a single-beat structure and its Fourier transform shows a frequency spread of 0.28–0.32 MG. After depinning the CDW at 1.1 K a more complex two-beat structure is observed as shown in Fig. 12(b). A MB model fit to this structure again requires a wider and more complex frequency distribution, similar to that required for the Fe_xNbSe_3 data of Fig. 10(b). This result is presented in Sec. IV.

The examples of beat structure shown earlier demonstrate the systematic connection between the metastable CDW structure and the variable amplitude modulation of the quantum oscillations. Although these metastable states and the associated beat structures are formed in fairly random fashion, the frequency and amplitude analysis shows a consistent behavior characteristic of the MB interference model discussed in Sec. IV. Increasing the impurity pinning also increases the magnitude and complexity of the beat structure, which is consistent with a direct connection between the pinned CDW structure and the local FS of the normal electrons.

We have also examined the magnetoquantum oscillations in the Hall resistance and correlated them with the simultaneous oscillations observed in the magnetoresistance. The results are reviewed below and provide additional evidence of the relation between the FS inhomogeneity generated by the pinned CDW structure and the quantum-oscillation amplitude and beat structure.

4. *Quantum oscillations and MB interference in the Hall resistance*

The Hall resistance has been measured in both the dc and ac modes at 1.1 K in a magnetic-field range of 0–230 kG. In this case a very large dc component of transverse voltage is measured, which shows a linear dependence on magnetic field as shown in the two curves of Fig. 13 for **H**‖**c** and Hall voltage ⊥**c**. These represent the two combinations of $\pm H$ and $+I$, and demonstrate that the lead configuration on this crystal introduces a negligible component of magnetoresistance. At 1.1 K the Hall effect is positive at all magnetic fields above ~1.5 kG; at the lowest fields a sign change is observed. The sign change plays an important role at higher temperatures and is discussed in more detail in Sec. III A 7.

The oscillatory component represents a smaller percentage of the total Hall voltage than observed for the magnetoresistance, but is easily detected and constitutes ~10% of the total voltage. The ac component obtained from a four-term sum of the $\pm I, \pm H$ set of ac curves is shown in Fig. 14(b). This curve exhibits the same basic low-frequency oscillations observed in the simultaneous recording of the magnetoresistance shown in Fig. 14(a). However, the frequency spread and beat structure are

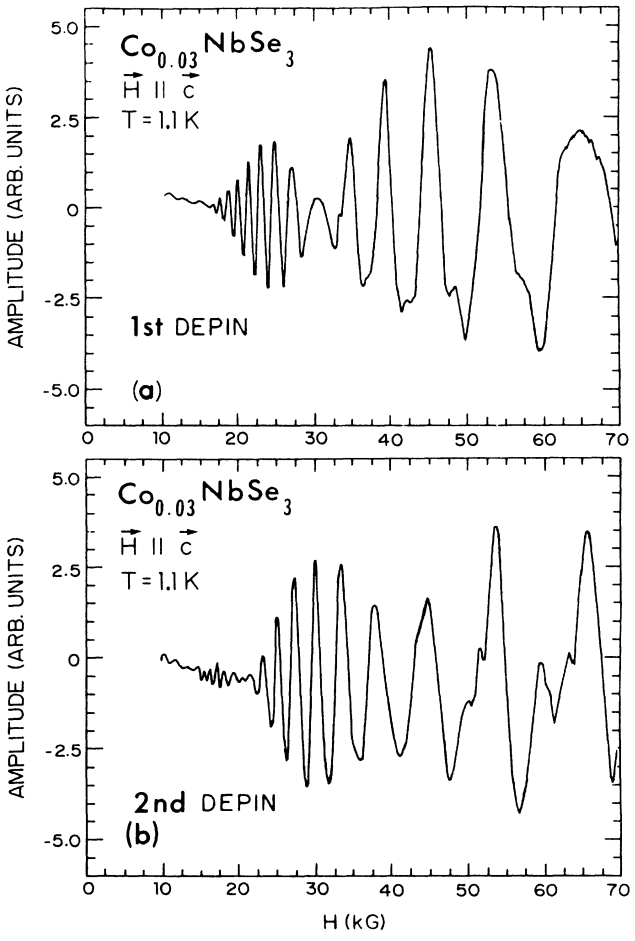

FIG. 12. Beat structures in the ac transverse magnetoresistance of a Co-doped $NbSe_3$ crystal grown from a powder of starting composition $Co_{0.03}NbSe_3$. In this case beat structures persist after repeated depinning and repinning of the CDW at 1.1 K. A single beat is observed in the curve of (a), while a more complex two-beat structure is observed in the curve of (b) recorded after a second depinning of the CDW at 1.1 K. These beat structures require rather complex frequency distributions in the model calculations and these are shown in Fig. 40.

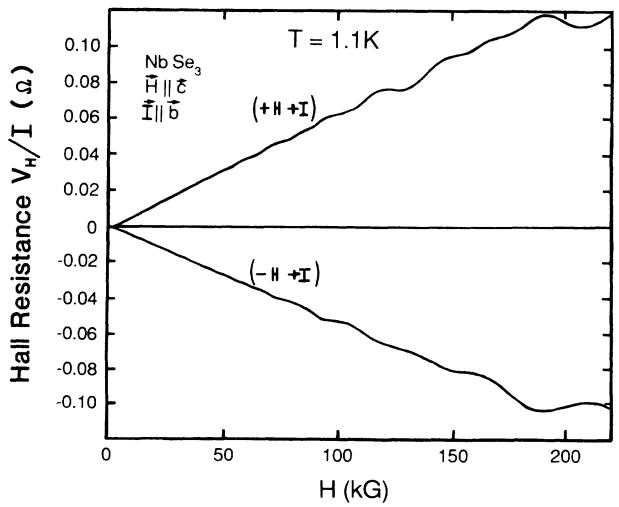

FIG. 13. dc Hall resistance measured at 1.1 K in the field range 0–220 kG. Curves are shown for ±**H** and +**I** and indicate the presence of little or no magnetoresistance component for this pair of Hall leads oriented perpendicular to **c**.

different, as shown in the Fourier transforms of Fig. 15. In the magnetoresistance the low-frequency peak is at 0.30 MG, while the Hall resistance shows a low-frequency peak at 0.29 MG. The frequency spreads are $\Delta F=0.06$ MG for the magnetoresistance and $\Delta F=0.09$ MG for the Hall resistance.

These variations suggest that different domains of CDW configuration and FS inhomogeneity contribute to the two resistivity components, as would be expected since the two measurements sample different regions of the crystal. The effects of depinning and repinning the CDW on the simultaneous measurement of the magnetoresistance and Hall resistance also give evidence supporting the aforementioned conclusion. The Fourier transforms of the ac data obtained after depinning and repinning the CDW at 1.1 K are shown in Fig. 16. As indicated in the transform of Fig. 16(a), the magnetoresistance shows a single low frequency of 0.28 MG, characteristic of most nominally pure crystals following CDW depinning. In contrast the simultaneously measured Hall resistance shows an increased frequency spread $\Delta F=0.10$ MG, as shown in Fig. 16(b), with a low frequency at 0.29 MG and a high frequency at 0.39 MG. This difference in FS inhomogeneity for the two measurements is consistent with the MB interference model. This is discussed in more detail in Sec. IV.

5. *Magnetoresistance in the 10–60 K range*

At $H=0$ the resistance at electric fields well below threshold shows a rapid increase with temperature above 10 K, which reaches a maximum at ~ 48 K and then decreases rapidly as the temperature approaches the CDW transition at $T_2=59$ K. If this resistance anomaly were

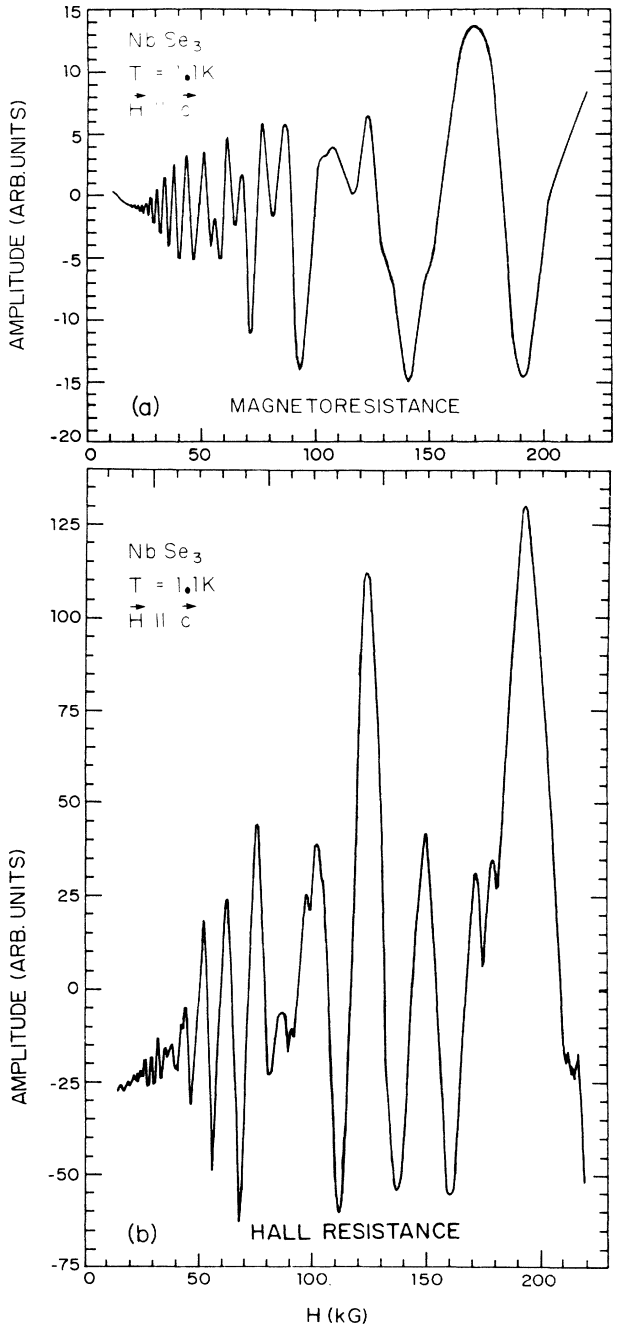

FIG. 14. Quantum oscillations observed simultaneously in (a) the magnetoresistance and (b) the Hall resistance in a pure $NbSe_3$ crystal in a field range 0–220 kG. The Hall resistance was measured perpendicular to **c** with **H**∥**c** and **I**∥**b**; $\mathcal{R}=220$. The oscillations were recorded in the as-cooled state before depinning of the CDW.

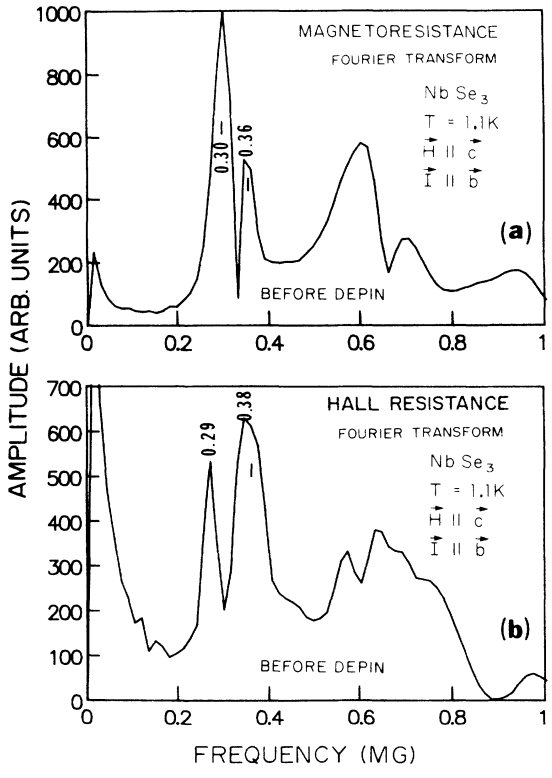

FIG. 15. Fourier transforms of the magnetoresistance and Hall resistance data shown in Fig. 14 for a pure $NbSe_3$ crystal. A large frequency split is observed in both components in the as-cooled state, but different maximum and minimum frequencies are present for each component. (a) magnetoresistance; (b) Hall resistance.

entirely due to FS obliteration below T_2 then ~60% of the FS existing above 59 K would have to be annihilated by gap formation in the low-temperature CDW phase. We have shown[4] that this low-temperature resistance anomaly is strongly enhanced by application of a magnetic field transverse to the **b** axis. At 227 kG the resistance is enhanced by up to a factor of 4 in the temperature range 59–10 K: this would require a FS annihilation below T_2 of 92% as opposed to 60% for $H=0$. In addition to the resistance enhancement the peak in resistance moves to lower temperature and is observed at ~38 K in a field of 226 kG.

This resistance enhancement is not associated with ordinary magnetoresistance, which is a function of the dimensionless parameter $\omega_c\tau$. The resistance enhancement does not change appreciably in magnitude with impurity doping, which reduces the $\mathcal{R}$ from ~200 to 20. In addition the magnetoresistance reaches an intermediate maximum at ~20 K, which is inconsistent with a dependence on τ. A scattering-time dependence should produce a monotonic increase as the temperature decreases in this range. Figure 17 shows accurate curves of the temperature dependence of resistance recorded at $H=0$ and $H=226$ kG in the temperature range 1.1–100 K for a $NbSe_3$ crystal with $\mathcal{R}=284$. In addition to the resistance enhancement the curves show an increase in T_2 of approximately 0.5 K in a field of 226 kG. Corrections have been made for the magnetic-field dependence of the carbon glass resistor used to measure the temperature, and the temperature controller has been carefully calibrated. However, an accuracy of better than ±0.5 K cannot be claimed for any single point, and a magnetic-field-induced increase in T_2 should be considered only a tentative result. The expected magnitude of any increase in T_2 is discussed in Sec. IV B 3.

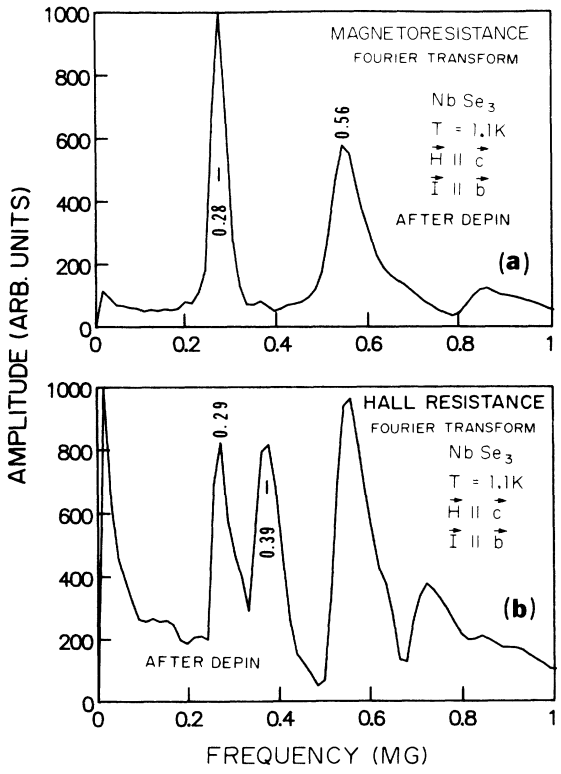

FIG. 16. Fourier transforms of the simultaneously measured magnetoresistance and Hall resistance recorded after depinning and repinning the CDW at 1.1 K immediately following the measurements presented in Figs. 14 and 15. (a) The Fourier transform of the magnetoresistance shows only a single low frequency of 0.28 MG plus a strong second harmonic of this frequency. (b) The Fourier transform of the Hall resistance continues to show a large frequency split, but different minimum and maximum frequencies are observed after depinning and repinning the CDW at 1.1 K.

The strong resistance enhancement by the magnetic field is observed for all field directions lying in the **a-c** plane. However, a considerable anisotropy is present as demonstrated in Fig. 18(a) for **H**∥**c** and **H**⊥**c** with $H=215$ kG. The resistance enhancement varies by approximately 30% between the two magnetic-field orientations; it is not unreasonable given the possible anisotropy of the FS. Figure 18(b) shows the resistance enhancement observed in an Fe_xNbSe_3 crystal at a field of 226 kG parallel to the **c** axis. Both the pure crystal of Fig. 18(a) ($\mathcal{R}=218$) and the Fe-doped crystal of 226 kG parallel to the **c** axis. Both the pure crystal of Fig. 18(a) ($\mathcal{R}=218$) and the Fe-doped crystal of Fig. 18(b) ($\mathcal{R}=31$) show almost identical enhancements, which indicates little or no dependence on residual impurities. The curves of Fig. 18 were not calibrated as carefully as the data of Fig. 17, and shifts near T_2 should be not be considered significant.

The large magnetoresistance described earlier is induced only by transverse magnetic fields and decreases smoothly as the field is rotated into a longitudinal orientation, as shown in Fig. 19(b) for $T=30$ K. The magnetic-field-induced resistance follows a $\cos\phi$ dependence, where ϕ is the angle between the magnetic field and the transverse orientation (⊥**b**). The component of **H** lying in the **a-c** plane is approximately parallel to the nested sections of FS and the magnetoresistance de-

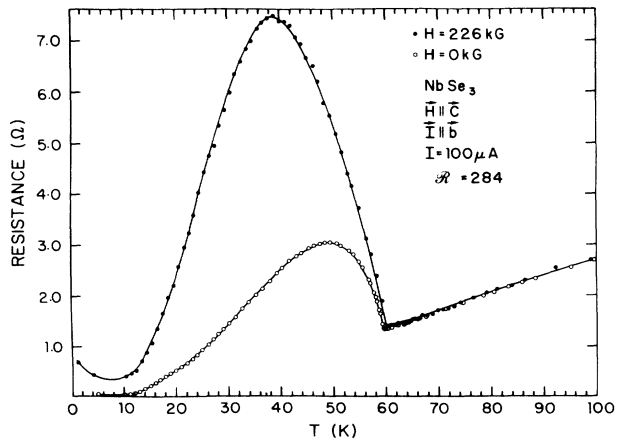

FIG. 17. The temperature dependence of resistance for a high-purity $NbSe_3$ crystal in the range 1.1–100 K. The curves show data obtained in zero magnetic field and in a transverse magnetic field of 226 kG. Below the CDW onset of ~60 K the magnetic field produces a large resistance enhancement and the CDW onset temperature is increased by ~0.5 K.

creases to a very small value as this component goes to zero at **H**||**b**. This behavior is consistent with the BF mechanism, which associates the enhanced magnetoresistance with a magnetic-field-driven change in the FS nesting. Only the transverse component of **H** should be effective: This model is outlined in Sec. IV.

6. *Hall effect in the range 1.1–60 K*

The dc Hall resistance in the static CDW state shows an unusual sign change as a function of magnetic field for **H**||**c** and **I**||**b**. At 1.1 K the Hall voltage changes from negative to positive at ~3 kG as shown in Fig. 20. For increasing temperature this zero crossing moves continuously to higher magnetic fields. The Hall voltage remains negative over the entire accessible field range for temperatures near T_2. Curves of Hall voltage versus magnetic field at $T=20$, 30, and 40 K are shown in Fig. 21. At the lowest temperatures the dc Hall voltage remains linear after the sign change, and corresponds to a net positive carrier density in the range $(5-8)\times 10^{18}/\text{cm}^3$ for $(\bar{p}-\bar{n})$, a magnitude consistent with a strong reduction in carrier density by formation of the two CDW's.

The magnitude of the Hall voltage at 1.1 K corresponds to a large transverse electric field, as compared to the longitudinal electric field. The calculated values of this field are quite variable because of the small transverse dimensions of the crystal (1–50 μm) and a high sensitivity to lead geometry. However, the ratios E_{xy}/E_{xx} are consistently in the range 25–100, indicating that the Hall angle is large and can approach 90°. This is also consistent with the presence of a large $\pm H$ asymmetry in some measurements of the magnetoresistance, even though the ratio of length between leads to crystal diameter is greater than 100.

At higher temperatures, in the range 20–50 K, the Hall voltage becomes nonlinear in both the negative- and positive-magnetic-field regions, and the magnitude relative to the magnetoresistance voltage is a more complex function of both the magnetic field and the temperature. In general, the Hall effect is sensitive to detailed changes in the carrier mobility, and reflects any changes in elec-

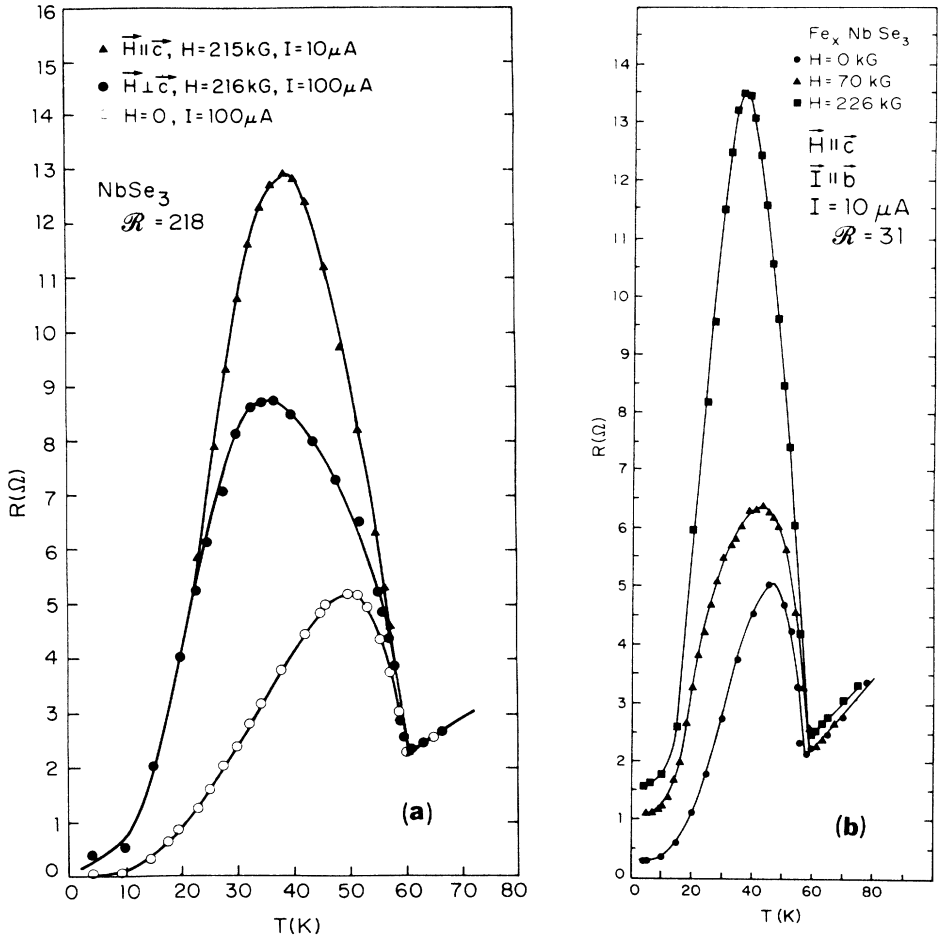

FIG. 18. (a) Comparison of resistance enhancement below the CDW transition in pure $NbSe_3$ observed for the transverse magnetic field of ~215 kG parallel and perpendicular to the **c** axis. The anisotropy in magnetoresistance is ~50%. (b) Effect of Fe doping the resistance enhancement in $NbSe_3$ induced by a transverse magnetic field of 226 kG parallel to the *c* axis. The magnitude of the enhancement in the Fe-doped crystal is comparable to that observed in pure crystal shown in (a).

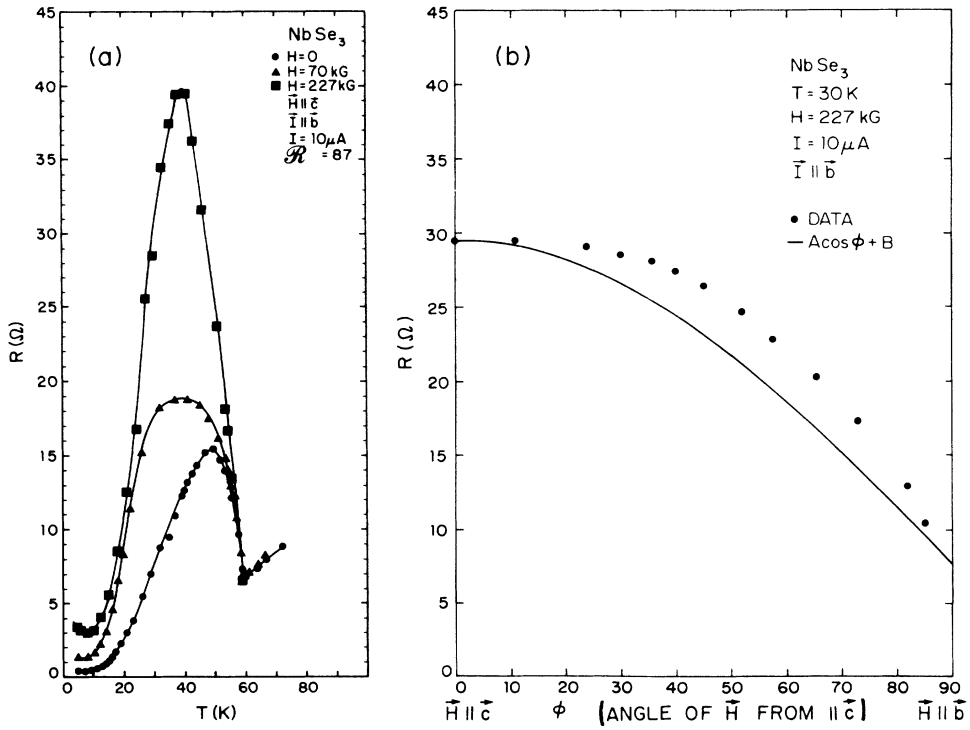

FIG. 19. Data showing the angular dependence of the magnetoresistance in pure $NbSe_3$ as the magnetic field is rotated from the transverse orientation parallel to **c** to the longitudinal orientation parallel to **b**. (a) Temperature dependence of resistance showing resistance enhancement induced by transverse magnetic fields of 70 and 227 kG parallel to **c**. (b) Resistance at 30 K in a magnetic field of 227 kG as a function of angle from the transverse orientation parallel to **c**. For **H**$\|$**b** the resistance enhancement decreases to zero.

tron to hole ratio, effective masses, or relaxation times. It must be related to mechanisms which enhance the magnetoresistance, but can present a more complex analysis problem. In the discussion further we consider the possible effects of the BF mechanism on the Hall voltage. It is certainly possible to generate a sign change in Hall voltage with the BF mechanism and we review a reasonable set of model parameters that can generate the Hall behavior at 30 K. Other mechanisms such as a low-field to high-field transition in one group of carriers can also produce a sign change in Hall voltage, although at present the experimental data and analysis do not provide any evidence for this mechanism.

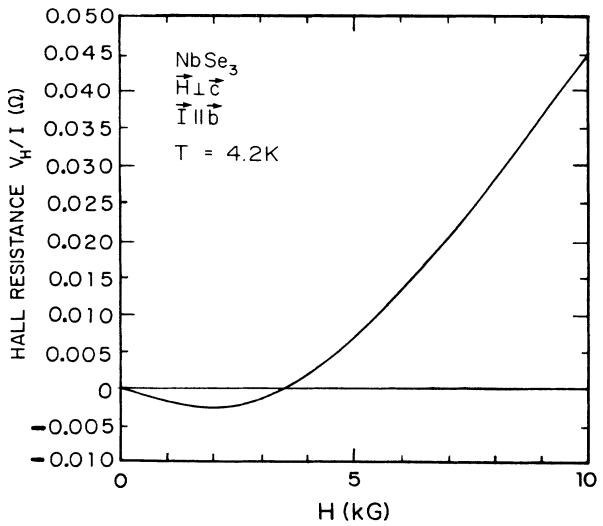

FIG. 20. Hall resistance of a pure $NbSe_3$ crystal measured at 4.2 K. Initial Hall resistance is negative, followed by a sign reversal at a magnetic field of 3.7 kG. The magnetic field is perpendicular to **c** with Hall voltage measured parallel to **c**; $\mathcal{R}=75$.

The Hall effect has also been measured in the nonlinear regime of CDW motion and again requires a rather complex analysis of the changes produced by CDW motion. The magnetoresistance is highly nonlinear in this region, and although the characteristic behavior can be well described by definite current-versus-voltage relations, the microscopic mechanisms are complex. We summarize the effects of CDW motion on magnetotransport in Sec. III B.

B. Nonlinear magnetotransport in the CDW motion regime

Both the magnetoresistance and Hall effect show nonlinear responses to motion of the CDW. As was the case for the static CDW state, the two different temperature ranges are dominated by different magnetic-field effects and respond differently to the CDW motion. We discuss the very-low-temperature regime first, where quantum oscillations are a major effect in the transport as measured in the range 1.1–4.2 K. The higher-temperature regime, from 10 to 60 K, is characterized by large nonlinear dc

terms due to the large fraction of total current carried by the moving CDW. The threshold electric field E_T and the impurity pinning are critical factors in this regime. We review results on nominally pure crystals with $\mathcal{R}$'s in the range 100–300 and on doped crystals with lower ratios and stronger pinning.

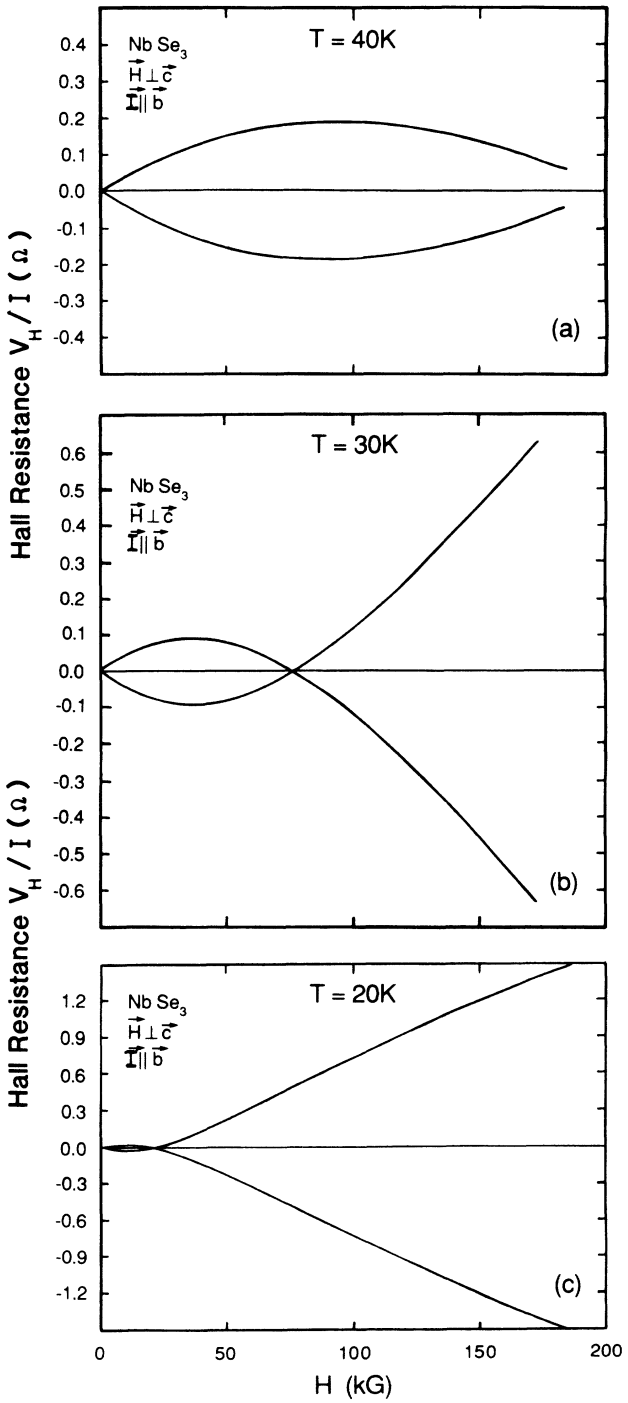

FIG. 21. Hall resistance of pure $NbSe_3$ ($\mathcal{R}=75$) as a function of magnetic field to 180 kG for three temperatures showing the monotonic increase in the zero crossing from 25 kG at 20 K to ~200 kG at 40 K. Two curves corresponding to $\pm H$ and $+I$ are shown for each temperature to demonstrate that the magnetoresistance component is negligible. Temperatures are (a) 40 K; (b) 30 K; (c) 20 K.

1. *Magnetoquantum oscillations in the presence of CDW motion*

The quantum-oscillation voltage amplitude and dc background voltage in a magnetic-field sweep are observed to increase with current according to Ohm's law until the electric field reaches the threshold for CDW depinning. For currents above threshold the oscillatory amplitude saturates while the overall voltage continues increasing, but exhibits a very nonlinear growth with current. Figure 22(a) shows a series of dc magnetoresistance curves recorded for a Ni_xNbSe_3 crystal in a magnetic-field range 0–220 kG and a current range from 1 to 100 mA. The threshold voltage for CDW motion in this crystal is ~35 mV at 1.1 K, and for currents above ~30 mA the field sweep curves enter the nonlinear region as indicated by the sharp voltage steps as the curves cross the threshold voltage for CDW motion. These curves can be fitted by the following current-versus-voltage relations:

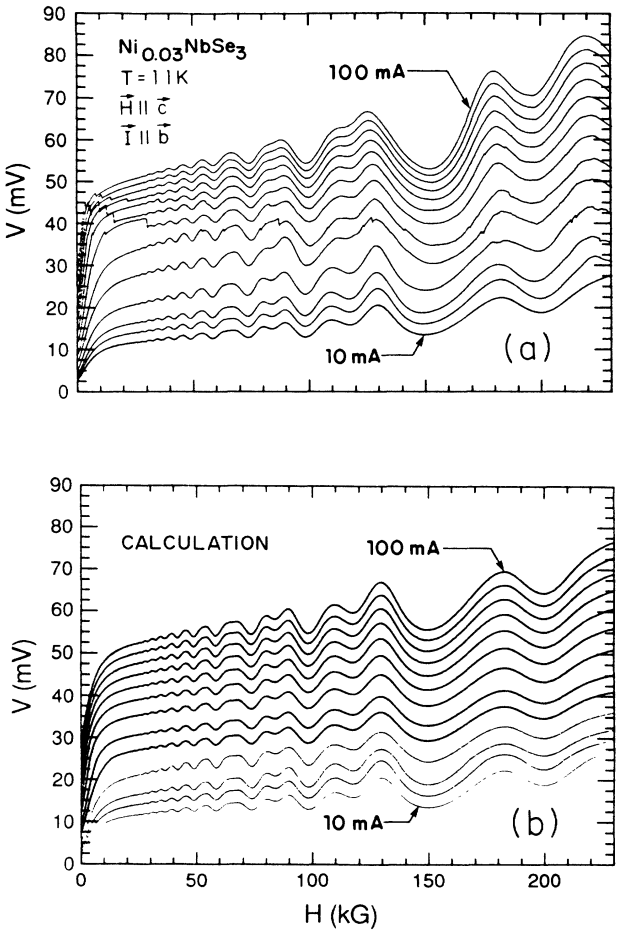

FIG. 22. (a) V vs H curves measured from a Ni-doped $NbSe_3$ crystal using a series of currents from 10 to 100 mA in increments of 10 mA. The magnetic field is parallel to c and is swept from 0 to 230 kG. (b) Model calculation of the V vs H curves using the functional relation given in Eq. (3.2). The fit is excellent and requires a large mixing of the normal and CDW quasiparticle components, as discussed in Sec. III B 1.

$$I=\frac{V}{R(H)} \quad (V<V_T)\,, \tag{3.1}$$

$$I=\frac{V}{R(H)}+\left[\frac{K}{R(H)}(V-V_T)\right]e^{-(V_0/V)} \quad (V>V_T)\,. \tag{3.2}$$

Here $R(H)$ and V are the measured resistance and voltage, V_T is the threshold voltage; K and V_0 are constants. The expressions used in Eqs. (3.1) and (3.2) follow the form used in the Bardeen tunneling model given in Eq. (3.3) later, except that they include an oscillating term in $R(H)$ and the constant K is introduced as a parameter. This should be viewed as an empirical fit and not a confirmation of the tunneling mechanism. The expression has sufficient parameters to give a very good fit to the data, but no microscopic interpretation of the parameters has been developed.

With $K=-11$ and $V_0=80$ mV a very good fit to the data is obtained [see Fig. 22(b)]. Expressions of this type can be developed from either the quantum-mechanical tunneling model[14] or the semiclassical model[15] used for CDW motion at $H=0$. However, in a magnetic field, oscillating components enter into the nonlinear term through the function $R(H)$. The oscillating component of this function would usually be associated with the normal electrons, but it also enters in the nonlinear term and generates an oscillation amplitude that is independent of current in the region of CDW motion. A detailed explanation for this experimental result involves a mixing of the normal quasiparticle and CDW components of the current and voltage.

2. *CDW motion effects on magnetoresistance in the range 10–60 K*

The CDW resistance anomaly that is enhanced by a transverse magnetic field responds to CDW motion in a similar fashion to that observed at $H=0$. The main difference is the large initial magnetoresistance prior to the onset of CDW motion. At high electric fields, with appreciable CDW motion the magnetic resistance approaches the resistance observed at $H=0$, as shown in Fig. 23 for $T=30$ K. The magnetoresistance in the large CDW motion state is very small, indicating that the moving CDW contributes little or no magnetoresistance.

The resistance in a magnetic field of 230 kG as a function of electric field shows this characteristic nonlinear behavior; examples in the temperature range 1.2–4.3 K are shown in Fig. 24. The data have been fitted using the Bardeen tunneling model[14] represented by the solid lines in Fig. 24, as calculated from the tunneling expression

$$\frac{R(E)}{R(0)}=\left[1+\frac{\sigma_b}{\sigma_a(H)}\left[1-\frac{E_T}{E}\right]e^{-(E_0/E)}\right]^{-1}, \tag{3.3}$$

where $\sigma_a(H)$ is the magnetoconductivity and σ_b is a magnetic-field-independent conductivity due to the tunneling channel; E_T is the threshold electric field and E_0 is related to the breakdown gap E_g and given by

$$E_0=\pi E_g^2/4he^*v_F\ ; \tag{3.4}$$

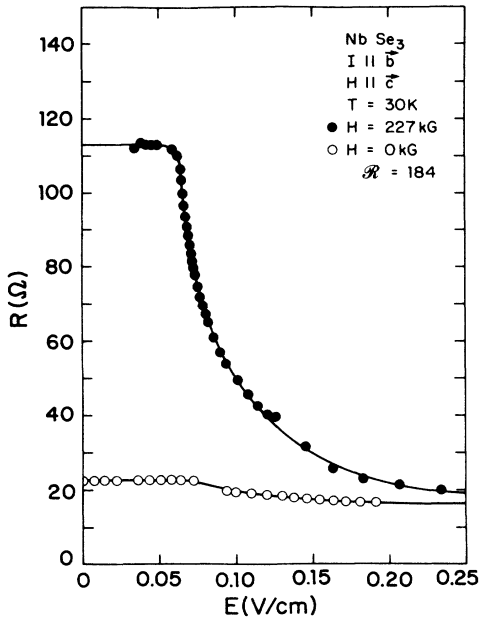

FIG. 23. Resistance vs electric field for a pure $NbSe_3$ crystal at 30 K in a transverse magnetic field of 227 kG and in 0 kG. The CDW depins at approximately 0.075 V/cm at both 0 and 227 kG. At high electric fields the magnetic-field-enhanced resistance is essentially eliminated by the CDW motion (Ref. 4).

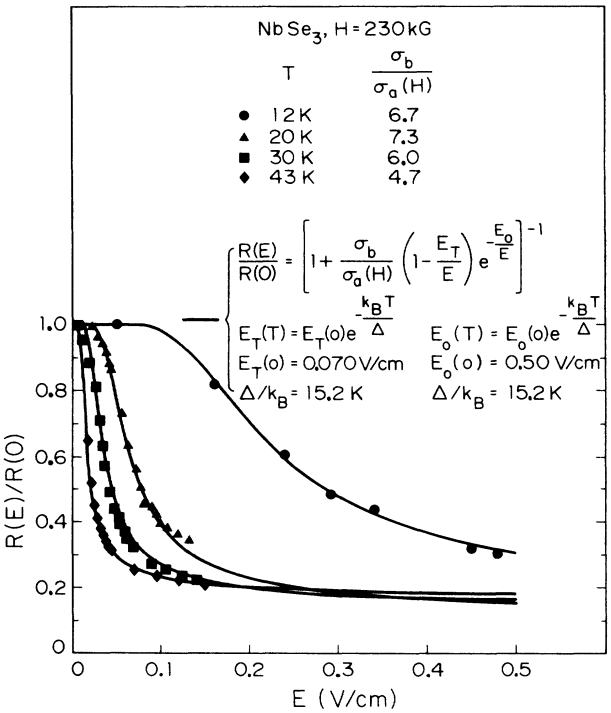

FIG. 24. The ratio of the resistance at electric field E to the resistance at $E=0$ as a function electric field for a pure $NbSe_3$ crystal in a transverse magnetic field of 230 kG. Curves are shown for four temperatures of 1.2, 20, 30, and 43 K. The solid lines are fits to the Bardeen tunneling model. Values of the parameters needed for the fits are listed in the figure. The values of E_T and E_0 used at each temperature have been calculated from the thermal-fluctuation model using values of E_T and E_0 at $T=0$, determined from the data shown in Fig. 25 [see Eq. (3.5) and (3.6)].

here h is Planck's constant, e^* is a parameter related to the effective charge and mass of the moving CDW, and v_F is the Fermi velocity. The use of Eq. (3.3) to fit the dc data at higher temperatures should again be viewed as empirical and not a confirmation of the tunneling mechanism. The expression in Eq. (3.3) allows a better parametrized fit of the data than the corresponding expression from the classical model, but the range of the data and interpretation of the parameters does not provide any clear confirmation of either model. The threshold electric field $E_T(T)$ and the parameter $E_0(T)$ have been self-consistently fitted, at four temperatures, using a thermal-fluctuation temperature dependence of the form

$$E_T(T)=E_T(0)e^{-k_BT/\Delta} \tag{3.5}$$

and

$$E_0(0)=E_0(0)e^{-k_BT/\Delta}, \tag{3.6}$$

where

$$\Delta/k_B=15.2\text{ K}.$$

As shown in Fig. 25 for a magnetic field of 206 kG, the thermal-fluctuation temperature dependence is accurately obeyed for the nominally pure specimens. The crystal used for the data of Figs. 24 and 25 had $\mathcal{R}=145$. The thermal-fluctuation behavior has been tested for other nominally pure crystals with $\mathcal{R}$'s in the range of 140–250, and is valid in most cases. The thermal-fluctuation behavior of E_T has been derived by Maki[18] and is discussed in Sec. IV B. In the case of impurity doping, strong deviations from the aforementioned behavior are observed. An example for Fe_xNbSe_3 is given in Sec. III B 5.

In a number of crystals the CDW motion at the lowest temperature of 1.1 K exhibits a sudden transition to a region of zero dynamic resistance. An example is shown in Fig. 26 for a very-high-purity crystal with $\mathcal{R}=284$. The region of zero dynamic resistance extends from 80 to 350 mA and is only limited by the current-carrying capacity of the contacts. This extreme nonlinear behavior occurs in relatively few crystals and it may be related to a specific configuration of strong pinning centers that depin suddenly at high electric fields. In the relatively high-ratio crystals the zero dynamic resistance is observed only at the lowest temperatures. The value of E_T observed at the lowest temperature in these samples is substantially higher than those obtained from extrapolation of the higher-temperature data. At high temperatures the nonlinear region also shows a finite dynamic resistance and follows the characteristic behavior described by the Bardeen tunneling expression,[14] as shown in Fig. 27.

In less pure crystals and in doped crystals regions of zero dynamic resistance can also be observed, but these are usually seen over a limited current range. In heavily doped crystals short regions of zero dynamic resistance can also be obtained at high temperatures; these have been termed switching crystals. Doping with Fe can in-

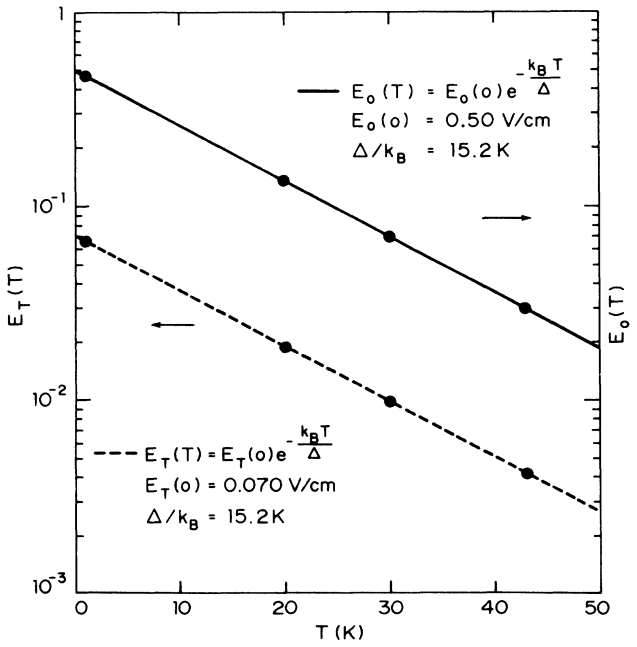

FIG. 25. Semilog plots of E_T and E_0 vs temperature in the range 1.1–50 K in a transverse magnetic field of $H=230$ kG parallel to c. The data points fit the expected thermal fluctuation model of Maki (Ref. 18) which has been used to determine self-consistently the values of $E_T(T)$ and $E_0(T)$ used for the tunneling-model fits shown in Fig. 24 in this sample; $\mathcal{R}=145$ [from Coleman *et al.*, Synth. Met. **19**, 795 (1987)].

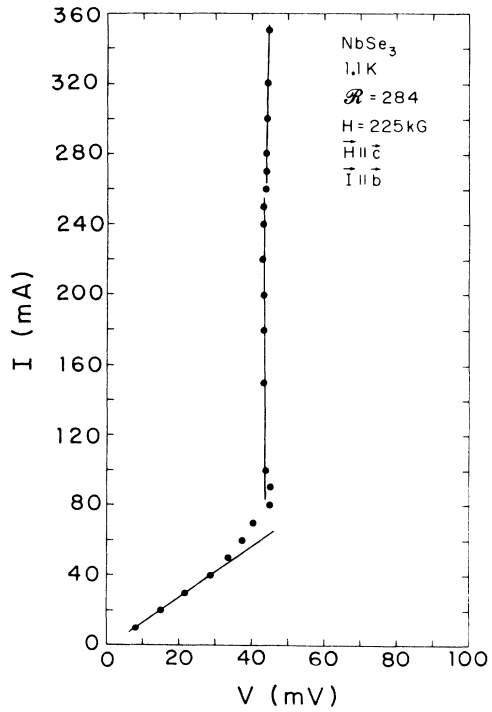

FIG. 26. Plot of I vs V at 1.1 K a pure $NbSe_3$ crystal in a transverse magnetic field of $H=225$ kG parallel to c; $\mathcal{R}=284$. After an initial nonlinear onset at ~35 mV the CDW motion exhibits zero dynamic resistance above ~45 mV [from Coleman *et al.*, Synth. Met. **19**, 795 (1987)].

duce such behavior in the range 20–30 K, as observed in both ac and dc experiments.[19]

3. *CDW motion effects on the Hall effect in the range 10–60 K*

The Hall effect has also been studied as a function of CDW motion and results for the magnetic-field range 0–200 kG are shown in Fig. 28(a) for H⊥c. At 30 K the threshold electric field is exceeded for a current between 1 and 5 mA. For increasing current the zero of the Hall voltage moves rapidly to higher magnetic fields.

The change in magnitude can be partly assigned to a change in the conductivity σ_{xx} along the axis of the crystal. If the only effect of CDW motion is a change in σ_{xx}, then $R_H\sigma_{xx}$=const, and R_H should decrease inversely with the increase of σ_{xx} as CDW motion occurs. This should change only the magnitude of R_H but not the magnetic-field value at which $R_H=0$. As shown in Fig. 28(b) the ratio of the Hall resistance to the resistance at $B=0$, as a function of current, is independent of current until the field exceeds ~30 kG. At higher magnetic fields the increased CDW motion changes the electron-hole balance contributing to the Hall voltage and thereby changes the zero crossing. This suggests that the same mechanism producing the enhanced magnetoresistance anomaly also contributes to the sign change in the Hall effect. Both features tend to be erased by large CDW motion at high electric fields. The BF mechanism discussed in Secs. IV A 3 and IV A 4, provides a possible explanation for the sign change observed in the Hall effect.

4. *CDW motion effects of the Hall effect in the range 1.1–4.2 K*

At liquid-helium temperature the sign change in the Hall voltage moves to extremely low magnetic fields (See Fig. 20). At 1.1 K we have measured the Hall voltage for magnetic-field directions both parallel and perpendicular to the c axis. The crystals are very thin perpendicular to the c axis and form ribbons with the wide dimension parallel to the c axis. The Hall gauge lengths parallel and perpendicular to c are 0.2–0.05 mm and 0.01–0.005 mm, respectively.

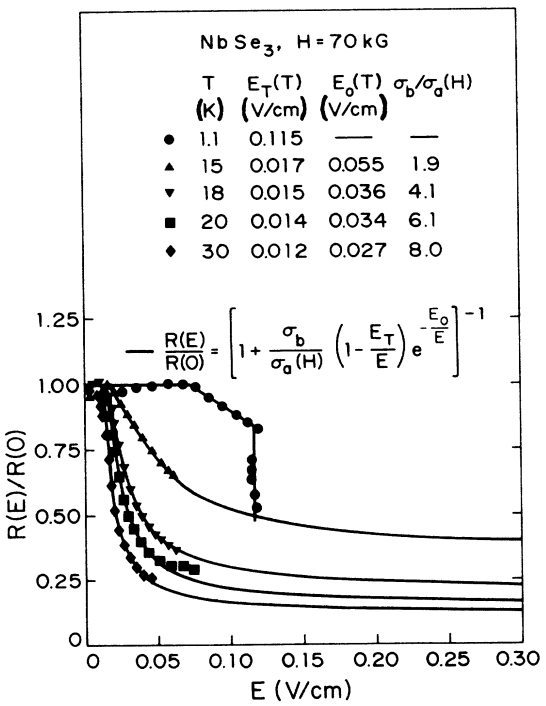

FIG. 27. Resistance vs electric field at five different temperatures in a transverse magnetic field of 70 kG parallel to c; $\mathcal{R}=284$. These data are from the same crystal as used for the measurement at 1.1 K in Fig. 26. A region of zero dynamic resistance is observed only at 1.1 K. At higher temperatures the Bardeen tunneling model provides a good fit as indicated by the solid lines. Values of the parameters are listed in the figure [from Coleman *et al.*, Synth. Met. **19**, 795 (1987)].

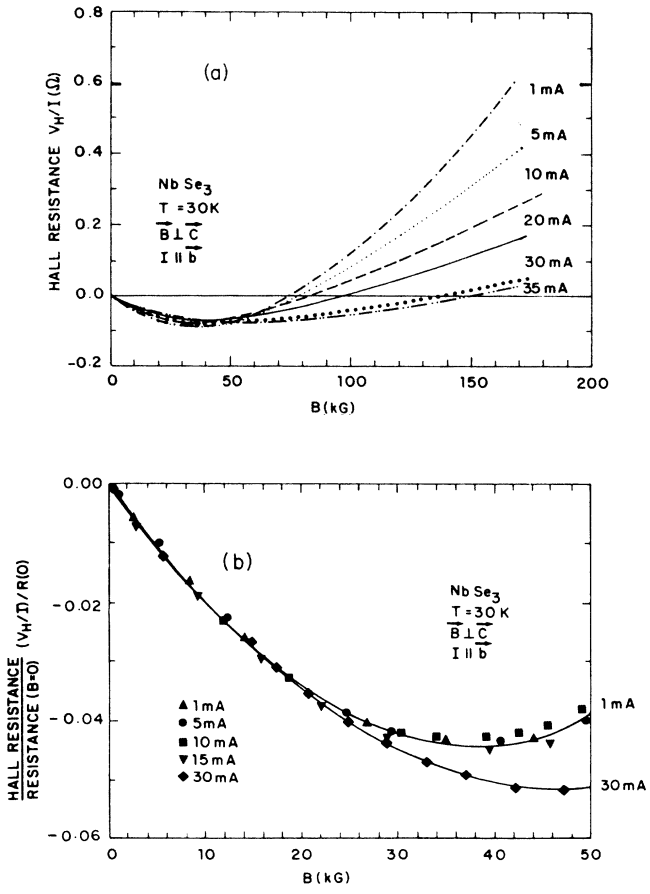

FIG. 28. The Hall resistance at $T=30$ K plotted as a function of transverse magnetic field for currents in the range 1–35 mA. (a) Magnetic-field range 0–200 kG. Increasing the current moves the zero crossing from ~75 kG at 1 mA to ~155 kG at 35 mA. (b) The data from (a) in the range 0–50 kG have been replotted by dividing the Hall resistance by the resistance at $B=0$. This corrects approximately for changes in σ_{xx} caused by CDW motion. The ratio is then independent of current up to ~30 kG, while at higher magnetic fields a more complex dependence on current (CDW motion) is still observed.

The effects of CDW motion on the Hall voltage in these two directions can be quite different. For H⊥c and Hall voltage measured parallel to c, the Hall resistance as a function of magnetic field in the range 0–70 kG is shown in Fig. 29(a) along with a simultaneous measurement of the magnetoresistance. Both decrease rapidly in the region of CDW motion and the ratio $[R(E)/R(0)]$ shows the same magnitude of decrease for each component. The true value of the Hall resistance requires correction for the effect of CDW motion on σ_{xx}, and other nonlinear terms may also be present at high magnetic fields. The Hall voltage is also sensitive to the number and configuration of CDW domains contributing to a particular measurement. The effect of CDW domain structure is also evident in comparing measurements of the Hall voltage in the two directions parallel and perpendicular to c. These two directions reflect the large anisotropy present in both the intrinsic atomic structure and crystal thickness. Measurement of the Hall resistance perpendicular to c, with H‖c, as a function of the electric field parallel to the b axis, is shown in Fig. 29(b). The data show simultaneous measurements at 1.1 K of the magnetoresistance and Hall resistance as a function of electric field in a magnetic field of 172 kG. In contrast to the measurement parallel to c, the Hall resistance perpendicular to c is independent of CDW motion, while the corresponding magnetoresistance shows the usual strong reduction above the threshold for CDW motion. These data were obtained in the same series of experiments where the quantum oscillations in the Hall voltage were measured for H‖c and $\mathbf{V}_H \perp$c, as presented in Secs. III A 4. The quantum-oscillation frequencies in the magnetoresistance and Hall resistance showed different responses to the CDW depinning and suggested that different domains of the CDW structure were dominating the two measurements. The direction ⊥c is also a direction of very low conductivity, since it is perpendicular to the layers of chains. At room temperature the conductivity anisotropy in the b-a plane was measured as ~500 compared to ~15 in the b-c plane. This large anisotropy in the conductivity and crystal structure may play a critical role in the CDW domain structure. If so it is more likely to show up in the measurements of the Hall voltage perpendicular to the chain slabs. Further discussion is given in Sec. IV.

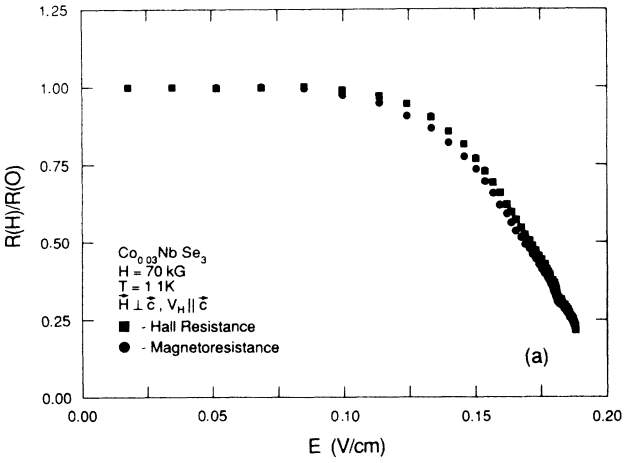

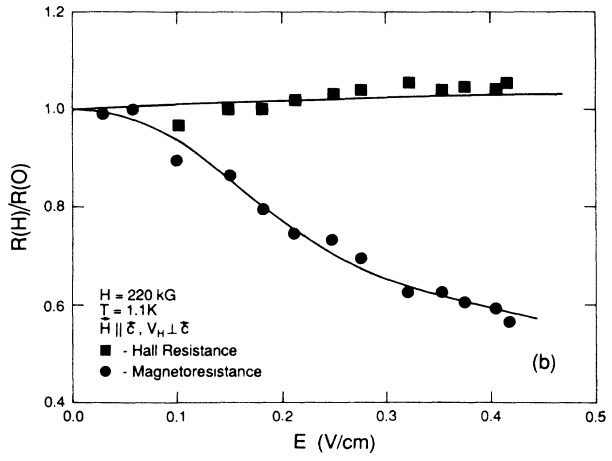

FIG. 29. Data show simultaneous measurements of the Hall resistance and the magnetoresistance at 1.1 K as a function of the longitudinal electric field for two different orientations of the magnetic field. The relative change from the resistance at low electric field (static CDW state) is plotted. (a) Magnetic field of 70 kG oriented perpendicular to c. Both the Hall resistance and magnetoresistance show a strong nonlinear dependence on CDW motion. (b) Magnetic field of 220 kG oriented parallel to c. The Hall resistance is independent of CDW motion, while the magnetoresistance shows a strong nonlinear behavior.

5. *Magnetic-field effects on the threshold electric field for CDW motion*

In the initial high-magnetic-field experiments[4,5] on $NbSe_3$ we previously reported observing a substantial reduction in the threshold electric field, E_T, required for CDW motion when a large transverse magnetic field was applied. We now believe that substantial magnetic-field-induced reductions in E_T are observed in random samples and result from specific aspects of the pinning configuration in a given specimen rather than from intrinsic modifications of the CDW condensate in a magnetic field. In general, the high-purity crystals show little or no change in E_T for the magnetic-field range 0–230 kG in the temperature range 10–60 K. In this temperature range thermal fluctuations dominate the behavior of E_T and any deviations occur only at very low temperatures. A measurement of E_T versus T for the highest purity crystal with $\mathcal{R}=284$ is shown in Fig. 30 for $H=0$ and $H=70$ kG. The values of E_T follow the thermal-fluctuation dependence at both $H=0$ and $H=70$ kG, with no change in the magnitude of E_T at a given temperature within the experimental accuracy of the measurement. The one point at 1.2 K corresponds to the zero dynamic resistance transition and represents a departure from the thermal-fluctuation behavior as well as the dynamic behavior observed at high temperatures.

The temperature dependence of E_T for H‖c and H⊥c

has also been measured on the relatively high-purity crystal with $\mathcal{R}=167$, and data at 70 kG are shown in Fig. 31 along with data at $H=0$. All curves again show the functional dependence characteristic of the thermal-fluctuation model. There is a small shift in the absolute values of E_T between the $H=0$ and $H=70$ kG curves, but all curves show the same value of Δ for the fit to the thermal-fluctuation model.

In less pure crystals both the temperature dependence of E_T and possible magnetic-field effects show a more complex behavior. These vary from sample to sample and would require an extensive series of experiments for complete analysis. Representative examples of the variable behavior introduced by changes in the impurity pinning are briefly described later.

The crystal doped with dilute concentrations of Fe were previously shown to have a wide distribution of FS deformations introduced by a more complex domain structure in the static CDW configuration (see Sec. III A 3). The behavior of E_T versus T for the Fe_xNbSe_3 crystals reflects the presence of a more complex pinned CDW structure that has completely modified the temperature dependence E_T, as shown in Fig. 32. In the range 40–25 K the values of E_T increase slowly and then show a sudden jump at 25 K. The threshold field E_T arises to a maximum at ~20 K and then decreases in the range 20–10 K. This behavior indicates a depinning process completely different from the thermal-fluctuation dependence observed for the nominally pure crystals. The same behavior is observed in a magnetic field of 70 kG either perpendicular or parallel to c, with no observable effect on the magnitude of E_T as also shown in Fig. 32.

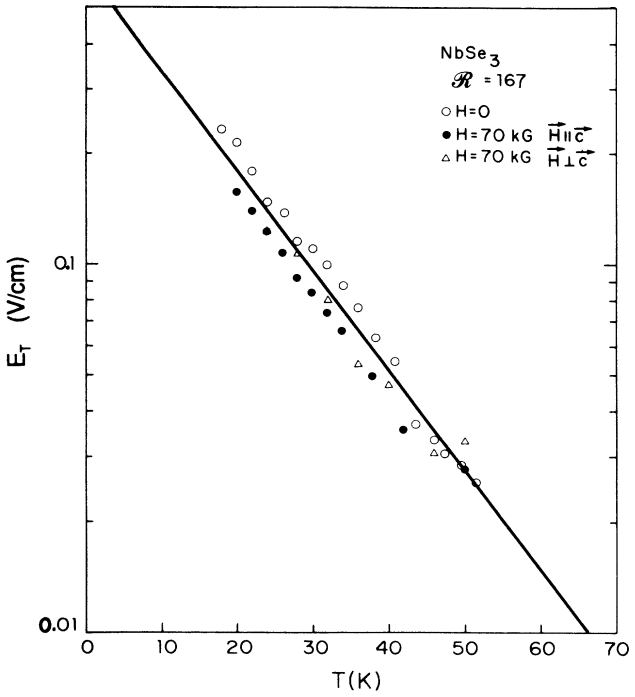

FIG. 31. Semilog plot of the threshold electric field, E_T, as a function of temperature for $H=0$ and $H=70$ kG, both parallel and perpendicular to c. Possible magnetic-field effects on E_T are zero within experimental error. The high-purity crystal with $\mathcal{R}=167$.

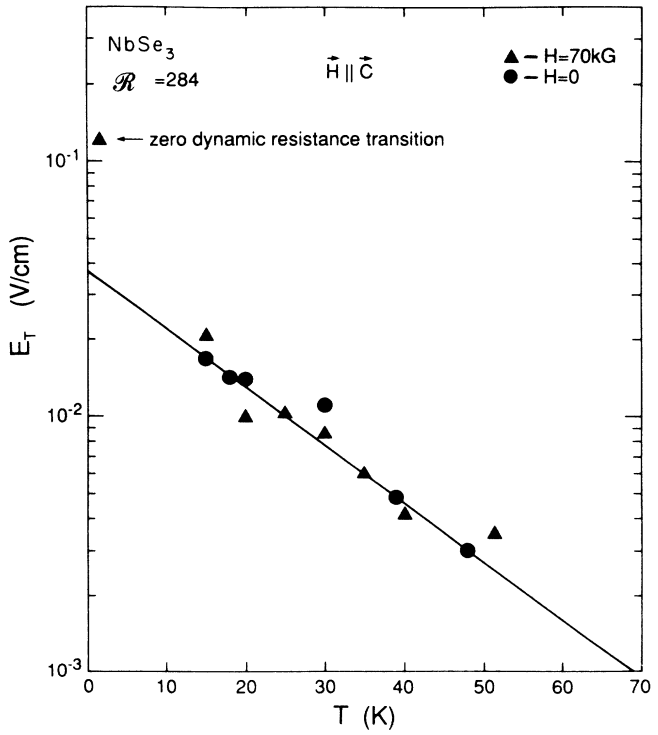

FIG. 30. Semilog plot of the threshold electric field, E_T, as a function of temperature for $H=0$ and $H=70$ kG oriented parallel to c. Data are from a high-purity crystal ($\mathcal{R}=284$) and no dependence of E_T on magnetic field is observed.

In the nominally pure crystals with $\mathcal{R}$'s in the range 100–200, the E_T versus T curves generally follow a

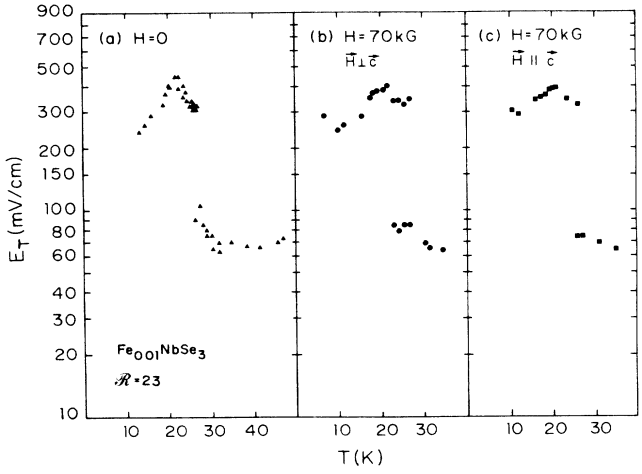

FIG. 32. Semilog plot of the threshold electric field, E_T, as a function of temperature for a crystal grown from $Fe_{0.01}NbSe_3$ powder measured at $H=0$ (a), and $H=70$ kG perpendicular to c (b), and parallel to c (c). In all three cases E_T shows a large discontinuous jump below ~25 K and a reversal of the temperature dependence below ~20 K. This temperature dependence is completely different from that observed for the pure crystals.

thermal-fluctuation behavior, and the resistance as a function of electric field shows a smooth nonlinear decrease reasonably described by the Bardeen tunneling-model expression.[14] For most crystals this characteristic behavior is observed over the entire temperature range 60–1.1 K. One exception already mentioned is the transition to the zero dynamic resistance state at 4.2 K and below. A second example of special behavior is shown in Fig. 33, where the low temperature magnetoresistance shows a large region of linear decrease with electric field followed by a sudden major depinning of the CDW. The threshold electric field at the end of the linear region is quite variable and can reach very high values, such as the 0.3 V/cm observed in the lower curve of Fig. 33(b). This behavior is not systematically related to $\mathcal{R}$ and indicates the presence of some special CDW configuration. The linear region also appears to be observed only in the presence of a transverse magnetic field as indicated in the upper curve of Fig. 33(a) for $H=0$.

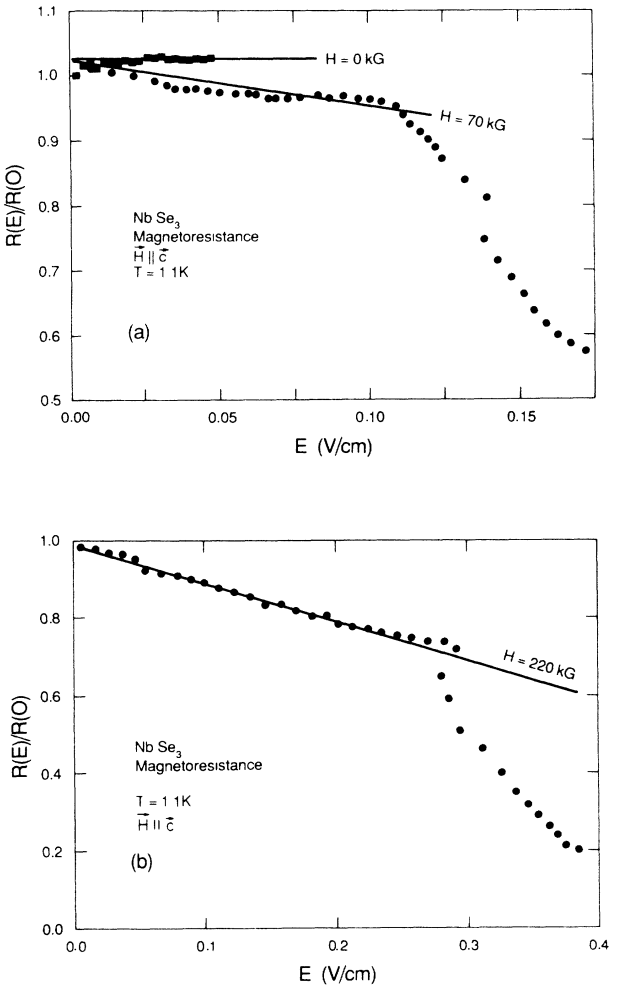

FIG. 33. Resistance of selected pure $NbSe_3$ crystals as a function of electric field in transverse magnetic fields of 0, 70, and 220 kG, showing region of linear decrease at 1.1 K induced by the magnetic field. Major CDW motion occurs at large electric fields. (a) $H=0$ and $H=70$ kG parallel to c; (b) $H=220$ kG parallel to c.

The preceding examples serve to indicate the variety of effects that can be observed in the dynamic CDW behavior when the impurity pinning increases from that observed in the highest purity crystals. Magnetic-field effects on the dynamic behavior of CDW motion needs to be analyzed with great care because of these variable effects; more experiments are required to sort them out.

IV. DISCUSSION

The experimental results summarized in Sec. III cover a wide range of responses to electric and magnetic fields that are observed in pure and doped $NbSe_3$ crystals. Some of these effects are related in a straightforward manner to modifications of electron transport in the presence of magnetic fields, while others require new mechanisms which have not been encountered in normal metals. These latter effects are directly connected to the CDW structure and the response of the FS to magnetic fields in the presence of CDW's. Two major effects involving different types of FS modifications have been proposed to account for the experimental results. One mechanism applies to the direct modification of the FS by the impurity pinning of the CDW, and is observed experimentally in the behavior of the quantum oscillations. The other mechanism is related to the magnetic-field-induced modifications of the energy spectrum at the Fermi level, and the associated change in the FS topology. As previously pointed out, these two effects become dominant in two different ranges of temperature, since one is a function of $\omega_c\tau$, while the other depends on $(\hbar\omega_c/\Delta)$. The former is only observable in the lower-temperature range, where τ is large, and is reviewed first.

A. MB model for magnetoquantum oscillations

We have previously used[9] a model describing MB in a one-dimensional open-orbit network in order to simulate the frequency shifts, frequency splitting, and amplitude modulation observed in the magnetoquantum oscillations of $NbSe_3$. This model was developed by Sowa and Falicov[10] to describe dephasing effects in MB; being a single one-dimensional open-orbit network, it exhibits MB and observable effects only in one direction.

A critical new feature in the model was the introduction of a stochastic distribution of small lens-orbit areas, resulting from FS deformation caused by the CDW. This effect can be viewed as a local shift in the Fermi level with resulting changes in both the local FS area and in the MB gaps. The variation in area was represented by a distribution in a MB phase θ, that could vary between limits θ_1 and θ_2, characteristic of the minimum and the maximum values of the **k**-space cross-sectional areas of the lens orbit.

For the present analysis we have extended the model to allow for magnetoresistance effects in two directions; the new version is still a one-dimensional network but it is enlarged by an additional, closed piece of FS and corresponds more closely to the actual case of $NbSe_3$. The

modified conductivity tensor is inverted to generate the dc magnetoresistance; the ac magnetoresistance is obtained by differentiation, which yields either $(d\rho/dH)$ or $(d^2\rho/dH^2)$ for direct comparison to the ac experimental data. The majority of the experiments measure the magnetoresistance along **b**, the direction perpendicular to the open orbits (that lie in the **a-c** plane of $NbSe_3$).

The model conductivity tensor, as given later, has two parts: one describing the open-orbit network and the MB interference, σ_{SF}, and an additional part describing the model closed-orbit contributions, σ_c. The total conductivity tensor perpendicular to the magnetic field is given by

$$\sigma=\sigma_{SF}+\sigma_c \ , \tag{4.1}$$

where

$$\sigma_{SF}=\frac{\sigma_0}{1+(\omega_c\tau)^2}\begin{bmatrix}1-Z_N/\omega_c\tau & -(\omega_c\tau-Z_N)\\ (\omega_c\tau-Z_N) & 1+\omega_c\tau Z_N\end{bmatrix}, \tag{4.2}$$

$$\sigma_c=\frac{\sigma_0}{1+(\omega_c\tau)^2}\begin{bmatrix}A & B\omega_c\tau\\ -B\omega_c\tau & C\end{bmatrix}. \tag{4.3}$$

The quantity Z_N is given by Sowa and Falicov,[10] and results from an evaluation of the effective path integral for the open-orbit network by means of an interpolation scheme for the intermediate-magnetic-field regime. The calculation computes the transmission and reflection coefficients at the junctions between the lens orbits and the arms of the open-orbit network, as shown in Fig. 34(a). The calculation follows the wave packet through the network as it undergoes repeated transmission and/or reflection at the MB junctions. Nonuniformity of the MB probabilities, caused by the interaction of the FS and the pinned CDW are included. Details can be found in Ref. 10.

The magnetic-field dependence of σ_{SF} exhibits interference phenomena arising from the nodes shown in Fig. 34(b). As the magnetic field is swept, various nodes in the network become nearly opaque because of destructive interference in the small lens orbits. Under these conditions the network becomes in fact a disconnected set of closed orbits and the magnetoresistance in all directions is dominated by the state of compensation (number of electrons versus number of holes) of the material. In the opposite limit, when the nodes are transmitting because of the constructive interference in the lens orbit, the open orbit dominates the transport properties and the magnetoresistance becomes extremely anisotropic.

The closed orbits corresponding to σ_c in Eq. (4.3) have been assumed to have the same relaxation time τ as the arms of the open-orbit network [Fig. 34 and formula (4.2)]. The contribution to the Hall conductivity, however, is taken to be the opposite sign: the closed orbits are holelike closed orbits. The new result is an uncompensated metal in which the magnetoresistance should very slowly saturate for very high magnetic fields, as observed in $NbSe_3$. The constants C and A in (4.3) are taken to be 4.0 and 0.2, respectively, which result in an anisotropy (for very low temperatures) of $(5.0/1.2)=4.17$ for the zero-field conductivity, a value not unreasonable for $NbSe_3$, where $\sigma_b/\sigma_c \simeq 15$ at room temperature. The constant B is taken to be 0.95 in order to balance (and almost but not completely compensate) the contribution from (4.2) and to fit the dc data.

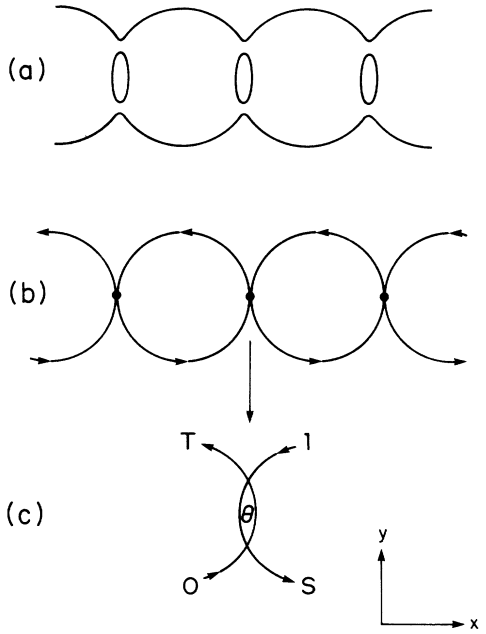

FIG. 34. (a) Linear open-orbit topology used to calculate the magnetic breakdown (MB) model. Breakdown can occur between the small lens-shaped FS sections and the open sections. (b) If the lens sections are very small, scattering can be neglected in calculating the MB interference. The model reduces to a breakdown vertex with transmission and reflection probabilities at each vertex along the linear chain. (c) Diagram of node connecting cells on the network. The parameter θ measures the phase corresponding to the lens area and T is the transmission coefficient with $S\equiv 1-T$ (from Ref. 9).

The conductivity tensor σ_{ij} is inverted to obtain the resistivity tensor ρ_{ij}. The diagonal component ρ_{22} parallel to the **b** axis is then computed numerically in order to generate curves for comparison to the experimental data. As shown in Fig. 35 the dc magnetoresistance generated in this way matches the experimental data quite well for a Ni_xNbSe_3 crystal in the range 0–220 kG. The model does not at present take into account the spin splitting, which becomes prominent at high magnetic fields. The derivatives $d\rho_{22}/dH$ and $d^2\rho_{22}/dH^2$ have been computed by direct differentiation of the ρ_{22} points generated by the model magnetoresistance tensor. The adjustable parameters are the frequency of oscillation, the frequency-distribution spread ΔF, and the critical magnetic-breakdown field parameter $\omega_0\tau$.

1. Model fits to the ac magnetoresistance

Calculated first and second derivative curves, which fit the ac magnetoresistance data of Fig. 8(a) for a Ni_xNbSe_3 crystal in the range 0–70 kG, are shown in Fig. 36. The beat structure is reproduced very well by the model and the frequency, and frequency distribution are essentially

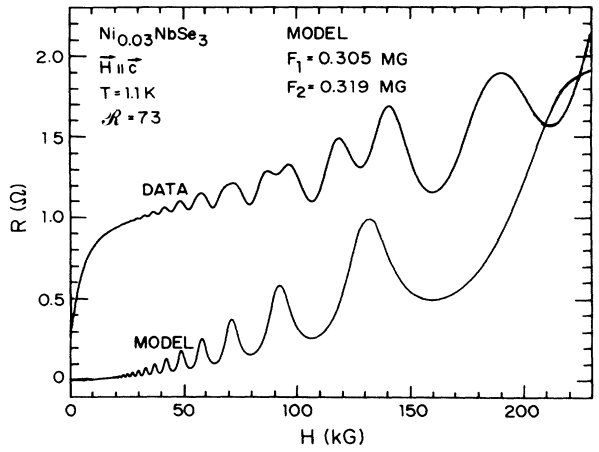

FIG. 35. Comparison of direct dc resistance data for a Ni-doped $NbSe_3$ crystal measured at 1.1 K in the magnetic-field range 0–230 kG and the resistance vs magnetic-field curve generated by the MB model using a frequency spread of 0.305–0.319 MG.

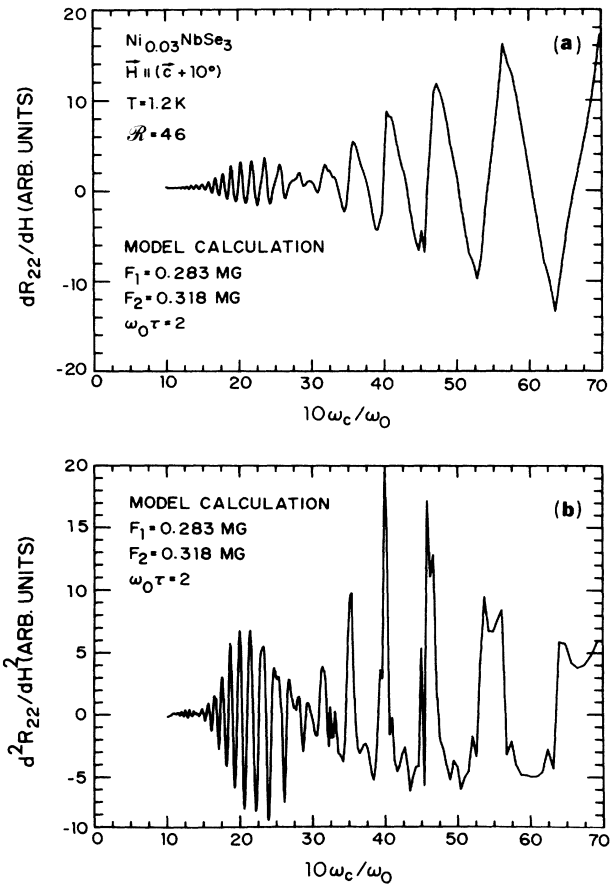

FIG. 36. First and second derivative curves obtained by differentiation of the dc MB curve generated to fit the Ni-doped $NbSe_3$ crystal used for the data of Fig. 8(a). The required frequency spread is very close to the experimental frequency spread determined in the Fourier transform of the data, as shown in Fig. 9(a). The model curves are plotted as a function of $10\omega_c/\omega_0$, where ω_c is the cyclotron frequency and ω_0 is the critical MB frequency. The scale corresponds to the magnetic-field values used in the experimental data curves and plotted in kG.

unique for this metastable CDW configuration. The experimental data can be recorded in either the first- or second harmonic mode. However, the data are usually taken in the second harmonic mode when the signal is large and the noise is low. Therefore, the calculated curves of $d^2\rho_{22}/dH^2$, such as that shown in Fig. 36(b), fit the amplitude envelope of the second harmonic experimental data more closely. In fact, comparison of Fig. 36(b) with the data of Fig. 8(a) shows that the amplitude envelope is essentially reproduced by $d^2\rho_{22}/dH^2$ versus H in the model calculation. However, as seen in Fig. 36(b), spikes and irregularities develop in the theoretical curves due to the great sensitivity of the calculational procedure to two successive differentiations. Suppression of this structure in $d^2\rho_{22}/dH^2$ requires excessive computer time. We have therefore used preferentially the calculated curves of $d\rho_{22}/dH$ versus H for comparison to experimental data. These first derivatives give the beat structure, frequency and frequency spread with the same accuracy, and are therefore sufficient for determining the main parameters of interest in the analysis. The first derivative curves are of course phase shifted by 90° from the second derivative curves, and this has been taken into account in the comparisons to experimental curves that are presented in the figures of Secs. III and IV.

The frequency distributions used to fit the data require that the lens areas show very different spatial variations for different metastable CDW states, particularly in the more heavily doped crystals. This feature is demonstrated for the sequence of ac magnetoresistance curves obtained for a Fe_xNbSe_3 crystal that were presented in Fig. 10 of Sec. III A 3. After the first cooldown the ac magnetoresistance showed a single large beat. The experimental curve is reproduced along with the calculated curve of $d\rho_{22}/dH$ in Fig. 37. The frequency distribution ranges from 0.283–0.321 MG and is shown in Fig. 38(a). In this distribution the amplitude rises rapidly above the minimum frequency, remains constant over most of the range, and decreases monotonically to the maximum. This particular distribution contains, in the numerical procedure, 40 equally spaced frequencies.

After the second cooldown the metastable CDW state is more complex, and gives rise to a greater range of frequencies and a nonuniform distribution. The experimental curve shows two beats with a modulated envelope of rather irregular shape. Figure 39 reproduces the experimental curve of Fig. 10(b) along with the model fit that reproduces the complex amplitude modulation quite well. The highly nonuniform distribution of frequencies required to fit the data is shown in Fig. 38(b). The minimum frequency is 0.275 MG, the maximum frequency is 0.345 MG, and three unequal frequency groups are required. This demonstrates the rather wide range of different deformed CDW metastable states than can be generated in the presence of fairly strong impurity pinning. These complex metastable states can be removed by depinning and repinning the CDW at 1.1 K, as was shown in Fig. 10(c). The model then fits the data with a single-group narrow frequency distribution extending from 0.280 to 0.284 MG, as shown in Fig. 38(c).

For Co_xNbSe_3 pinning and repinning the CDW at 1.2

K creates a more complex array of metastable CDW domains. Figure 40 shows four different distributions that result from successive depinning of the CDW at 1.2 K. The quantum-oscillation data shown in Figs. 12(a) and 12(b) required the calculated frequency distributions shown in Figs. 40(b) and 40(d), respectively. In all four metastable states the low end of the frequency distribution extends down to 0.26 MG, a value lower than previously required either in the pure crystals or in the Fe- and Ni-doped crystals. This may indicate an overall shift of the FS by the Co impurity. The complex beat structure observed in Co_xNbSe_3 and the persistence of a fairly complex frequency distribution after several depinning sequences suggests that the CDW interaction with the Co impurity is quite strong.

2. *MB process and MB gap*

The MB mechanism and orbit topology proposed in the analysis given here involves breakdown between the normal FS pockets and the open orbits that exist on the open sheets of the FS responsible for the nesting and the formation of the CDW. The gap involved in the MB is therefore Δ(CDW) and exists at the "zone" boundaries of the superlattice of the low-temperature CDW phase. The small lens orbits could exist on a closed pocket arising either from imperfectly nested FS sheets or from the one unnested band. In either case the structure is refolded into the super zone of the CDW and the resulting topology could easily be that of multiply connected "undulating cylinders" or "corrugated planes" intermingled with small pockets of holes and electrons embedded in them. Analysis of the angular dependence of the quantum-oscillation frequency suggests that the lens orbit arises from an elliptical FS pocket of principal axes with ratios 1:2.5:8.6 along the **b**, the perpendicular to **c**, and the parallel to **c** crystal axes, respectively. The ratio of the volume of this pocket, V_{pk}, to the volume of the BZ, V_{BZ}, is 1.2×10^{-3}. The effective mass of the carriers in this pocket can be calculated[16] from the temperature dependence of the oscillation amplitude and yields $m^*=0.24m_e$.

The magnetic breakdown probability is

$$P=\exp\left[-\frac{H_0}{H}\right]\equiv\exp\left[\frac{-\pi c\Delta_{\mathrm{CDW}}^2}{4\hbar|e|H|V_xV_y|}\right]. \quad (4.4)$$

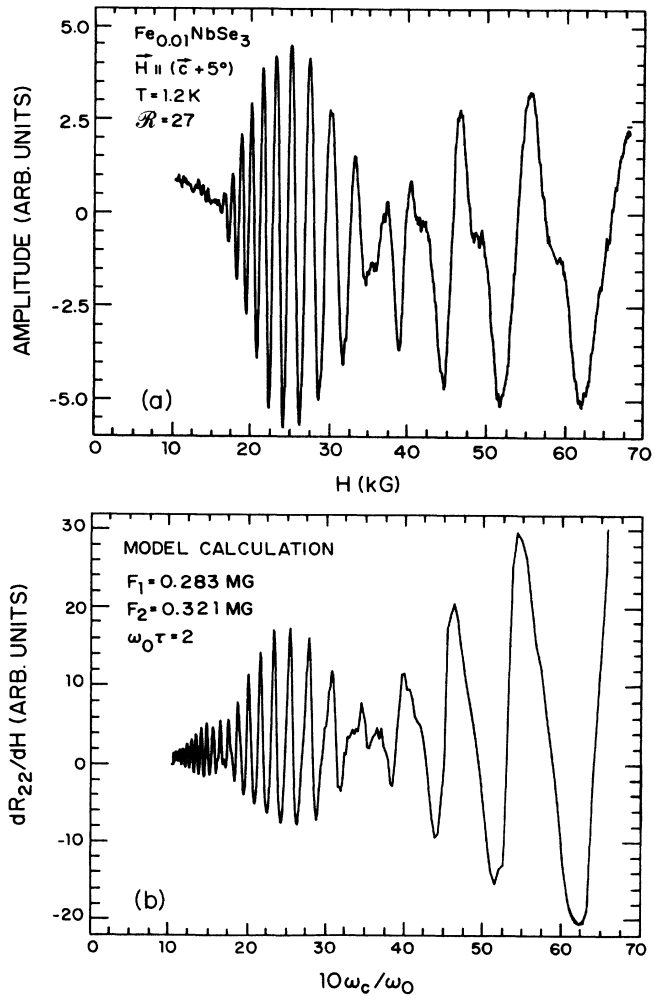

FIG. 37. (a) ac magnetoresistance data recorded from an Fe-doped $NbSe_3$ crystal at 1.2 K in the as-cooled state and showing a strong beat structure. (b) MB model fit generating the same beat structure shows a frequency spread from 0.283 to 0.321 MG.

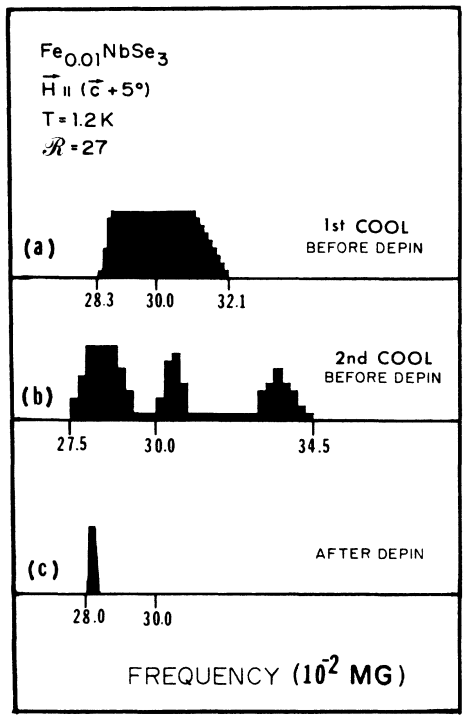

FIG. 38. Frequency distributions generated by the MB model that are required to fit the data recorded from an Fe-doped crystal and presented in Fig. 10. The maximum and minimum frequencies are in good agreement with the direct Fourier transforms of the data shown in Fig. 11. (a) First cooldown before depinning the CDW. (b) Second cooldown before depinning the CDW. (c) After depinning and repinning the CDW at 1.2 K.

To estimate the value of Δ_{CDW} we take

$$V_x V_y \simeq \frac{\pi}{4}\frac{\varepsilon_F}{m^*}$$

and use

$$\Delta_{CDW} = \left[H_0 \varepsilon_F \frac{|e|\hbar}{m^* c} \right]^{1/2} . \tag{4.5}$$

With $H_0 = 5\times 10^3$ G, $\varepsilon_F = 0.37$ Ry, and $m^* = 0.24 m_e$, we obtain $\Delta_{CDW} = 24.5$ meV. This value is not unreasonable, and should be compared to values of 35 ± 5 meV and 20–25 meV obtained from tunneling experiments.[20,21]

Variations in the size of the lens orbit are associated with domains of the CDW, where deformation of the CDW by impurity pinning has reduced the CDW gap and the CDW amplitude, thereby changing the Fermi level within the domain and increasing the size of the FS pocket. Such domains should have a characteristic length equal to or greater than the mean free path of the electron in order to allow for coherence in the magnetoresistance contribution from each domain. The exact domain configuration must necessarily be a complicated function of the impurity distribution, crystal perfection, surface structure, etc., as well as of the random pinning configuration obtained after each cooldown or application of a large electric field. The simultaneous measurement of the ac Hall oscillations and the magnetoresistance oscillations showed that the contribution to the two measurements come from different domains, and that various domain distributions yield therefore different results for the two measurements. The presence of a greater frequency spread that persists in the Hall data might be interpreted to mean the presence of strongly deformed domains at the crystal surface that contribute more to the Hall effect than to the magnetoresistance; the latter averages over the entire crystal volume. Further experiments are underway to test for the presence of domains using multiple sets of magnetoresistance leads along the length of the crystal. Initial results show the existence of different FS distributions along different lengths of the crystal. These results will be reported in a separate publication.

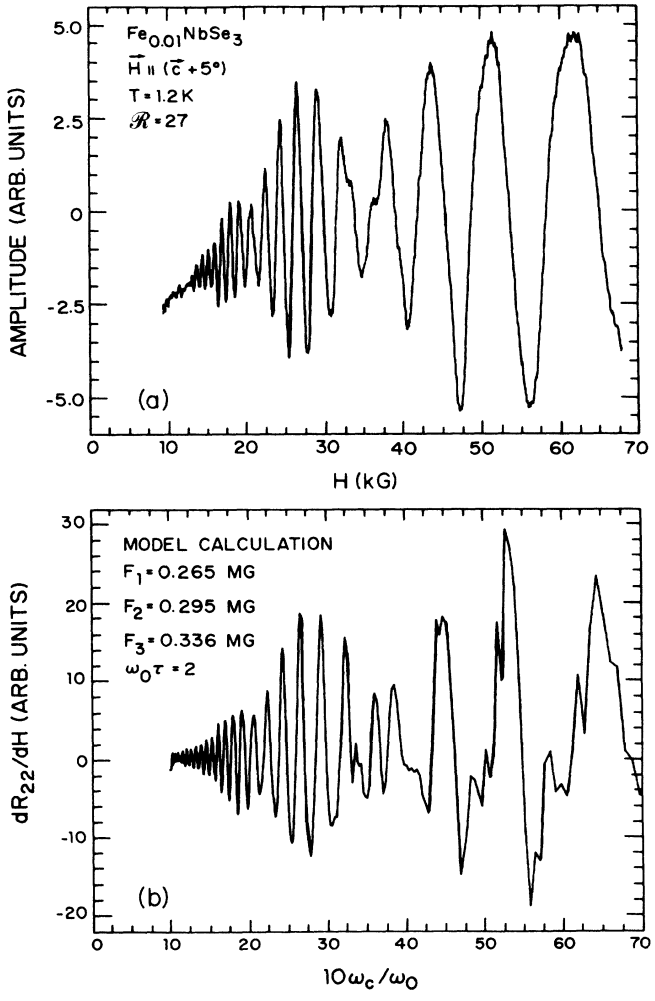

FIG. 39. (a) ac magnetoresistance measured at 1.2 K for an Fe-doped $NbSe_3$ crystal. [Replot of the data of Fig. 10(c) and fitted by the frequency distribution shown in Fig. 38(b).]. (b) The MB model fit with a complex three frequency group, shown in Fig. 38(b), does a good job of reproducing the observed magnetoresistance curve.

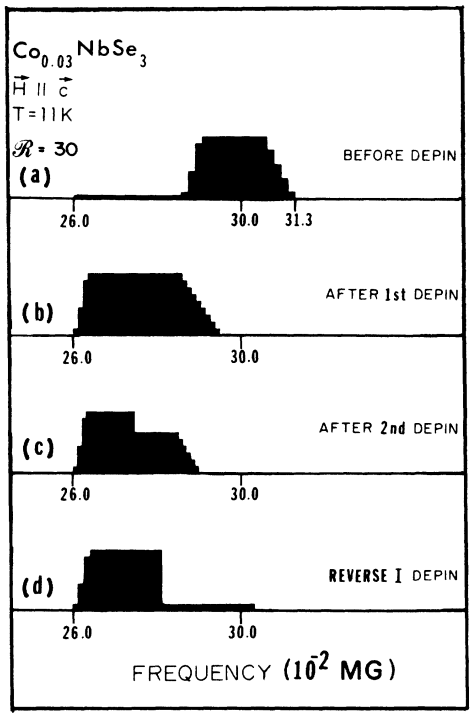

FIG. 40. Frequency distributions required to fit the MB model to a series of ac magnetoresistance curves recorded from a Co-doped $NbSe_3$ crystal. The frequencies are shifted substantially by a sequence of depinnings and repinnings of the CDW, but a single low frequency cannot be reached. In addition the lowest frequency of 0.26 MG is lower than observed in either the nominally pure, or Ni- and Fe-doped crystals. (a) Initial as-cooled state; (b) first depinning and repinning of the CDW; (c) second depinning and repinning of the CDW; (d) depinning and repinning of the CDW using a reversed current direction.

B. Magnetic-field-induced modifications of the CDW structure in $NbSe_3$

At higher temperatures the electron-phonon scattering rises rapidly and the large amplitude magnetoquantum oscillations proportional to $\omega_c\tau$ are no longer dominant above ~ 10 K. At temperatures in the range 10–59 K both the static and dynamic CDW contributions to the magnetotransport are influenced by the magnetic field, but in this case they derive from direct modifications of the FS by the magnetic field rather than from indirect FS modifications associated with the pinning of the CDW. The pinning by impurities remains important for the determination of the threshold electric field E_T, but the magnetic field appears to have relatively small effects on the depinning process at high temperatures. The magnetic-field experiments at higher temperatures indicate that the critical parameter is the ratio of the cyclotron energy, $\hbar\omega_c$, to the charge-density-wave gap, Δ_{CDW}. The analysis used to explain a number of the magnetotransport effects is summarized in the following sections.

1. Enhanced magnetoresistance in the 10–59 K range

The large magnetoresistance observed for magnetic fields transverse to the **b** axis in the temperature range 10–59 K requires an unusual mechanism not found in normal metals. The enhanced magnetoresistance develops below the CDW onset of $T_2=59$ K and is connected to the modifications of the FS produced by the CDW. Since no magnetoresistance enhancement is observed at temperatures above 59 K, where only the higher temperature CDW is present, there is a strong indication that the imperfect nesting of the FS sheets connected with the low-temperature CDW plays a critical role in the required mechanism.

In quasi-one-dimensional materials exhibiting a spin-density-wave (SDW) phase it has been known for some time that a magnetic field applied perpendicular to the axis of high conductivity (parallel to the open FS sheets) can enhance or induce a SDW. Gor'kov and Lebed[22] gave the first theoretical interpretation of this effect and Hériter *et al.*[23] have generalized the theory to include the magnetic-field dependence of the **q** vector of the SDW. In materials such as (tetramethyltetraselenafulvalene) $(TMTSF)ClO_4$ this leads to a cascade of SDW phase transitions which produce the unusual oscillations of the magnetoresistance observed in this material at very low temperatures.

In general a SDW system would be expected to couple more strongly to a magnetic field than a CDW system. However, Friedel[24] has argued that magnetic-field effects on the open sheets of a nested FS should be observable for both SDW's and CDW's. In the original report on the observation of a large enhancement of the dc magnetoresistance in $NbSe_3$ by Coleman *et al.*[5] it was suggested that a SDW component of the density wave in $NbSe_3$ might account for the effect, although no direct evidence was available. The authors concluded that either the number or mobility of the normal electrons is decreased by the magnetic field.

Based on the observed reduction of conductivity in a field of 227 kG it was estimated that an additional 92% of the FS area was removed by the CDW transition at 59 K versus 60% at $H=0$. These numbers are based on a simple model assumption and do not allow for changes in effective mass, mobility, scattering, topology, or other factors which contribute to the complex transport properties in $NbSe_3$. One would expect the total number of normal carriers to decrease if the FS area or topology were substantially changed by a field-induced increase in nesting, while the number of carriers in the CDW condensate would increase. However, any quantitative estimate can only be made from indirect measurements, such as narrow-band noise as a function of magnetic field, and at present estimates from these experiments are uncertain.[25,26]

Balseiro and Falicov[6] have considered the problem of the magnetic-field effects in a quasi-one-dimensional semimetal in the presence of a stable CDW or SDW. The density-wave (DW) state is characterized by imperfectly nested FS sheets which produce small electron and hole pockets of normal electrons in addition to the DW condensate. The DW causes gaps in an otherwise continuous spectrum, while the magnetic field quantizes the electronic motion in the two directions perpendicular to the magnetic field. This quantization tends to form either discrete levels and narrow bands if the cyclotron orbits are closed, or complicated continua if they are open. As the magnetic field is increased from zero, the competition between these various effects can cause very complex behavior which substantially modifies the energy spectrum near the Fermi level.

The usual Onsager quantization rules, applicable at relatively low magnetic fields, neglect several secondary effects such as band broadening, tunneling between bands, and the complicated structure of the continuum. These effects can be quite important in the presence of a DW when the cyclotron energy $\hbar\omega_c$ of the closed electron or hole orbits of the same order as Δ, the gap parameter characterizing the DW.

For intermediate and high magnetic fields, there is a substantial broadening of all Landau levels. This very large broadening of the Landau levels, in particular the $n=0$ levels, and the existence of gaps in the semiclassical continuum can be understood only in terms of a magnetic-field-induced mixing of the electronic bands. This mixing is important if the magnetic cyclotron energy $\hbar\omega_c$ is of the same order of magnitude of the gap parameter Δ.

For high magnetic fields the energy spectrum can show a large gap at the Fermi level, resulting in an insulating system. This central gap $2\Delta_g$ is of the order of 2Δ. As the magnetic field is reduced, the size of the insulating gap decreases and vanishes for a given value of the field which depends on Δ. For magnetic fields smaller than this value, there is a band of allowed continuum states at the center of the spectrum; the system is semimetallic.

The appearance of the Fermi-level gap would produce a semimetallic to semiconducting transition if the FS consisted only of the electron and hole pockets generated by the imperfectly nested FS sheets. If other FS sections are present the conductivity would decrease toward a

minimum value as the subset of electrons and holes shrink in response to a "more perfect nesting" induced by the magnetic field.

As previously stated, the large conductivity change observed between 0–227 kG would require an area shrinkage of these pockets of at least 80%, based on a conductivity change caused exclusively by a change in the FS area. The quantum oscillations observed at lower temperatures show no such large area change as a function of magnetic field, leading to the conclusion that the oscillations must arise from an additional section of FS, one which is not strongly modified by the magnetic-field-induced "more perfect nesting."

The general picture then is one of a complex FS involving a number of small pockets with a substantial range of effective masses. Some of these are modified extensively by a magnetic-field-driven improvement in the FS nesting, while at least one pocket is not. This behavior leads to a magnetoresistance that rises fairly rapidly in the field range 0–150 kG and then tends toward saturation above 200 kG.

The Balseiro-Falicov model provides a plausible framework for the behavior of $NbSe_3$ in the intermediate temperature range of 10–59 K. The electron and hole pockets in question are not seen in the quantum-oscillation regime at low temperature, suggesting that they have either very heavy masses or are quite large with corresponding low $\omega_c\tau$ values relative to those of the observed pocket. The one small pocket dominating the quantum-oscillation regime would therefore be assumed to have a much lighter mass (measured as $0.24m_e$) (Ref. 16) and much higher $\omega_c\tau$ values—in the range 1–10–for the present experimental magnetic-field range. The small pocket must be connected by MB to the nested open FS sheets, but need not be part of the same band.

If the pockets of holes and electrons arising from the imperfectly nested sheets of FS can dominate the higher-temperature dc magnetoresistance, then they would certainly be expected to influence the Hall effect. We discuss briefly a simplified model in Sec. IV B 2.

2. *Magnetic-field-induced sign change in the Hall effect*

In general the magnetic-field dependence of the Hall effect in systems with open orbits and/or MB can result from a complex set of contributions and is not susceptible to easy analysis. However, a simplified model of the Balseiro-Falicov mechanism can qualitatively produce the observed sign change of the Hall effect if it is assumed to result from the electron and hole pockets associated with nesting. A summary of the pertinent results is given later.

The effects of the Balseiro-Falicov mechanism on the Hall effect can be examined in a simple model of spherical hole and electron pockets with conductivities of the form $\sigma=Ne^2\tau/m$. If τ_h and τ_e are taken to be equal, and equal to τ, the Hall resistance in the low-field limit is given by

$$\rho_{12}=\frac{H[(N_h/m_h^2)-(N_e/m_e^2)]}{|e|c[(N_h/m_h)+(N_e/m_e)]^2} . \tag{4.6}$$

As the magnetic field is increased, the improved nesting removes normal carriers in both the hole and electron pockets. We can define this reduction factor by a function $X(H)$ such that

$$\begin{aligned} &N_e\rightarrow N_e[1-X(H)] , \\ &N_h\rightarrow N_h-\gamma N_e X(H) . \end{aligned} \tag{4.7}$$

Here we take $\gamma=1$ for the sake of simplicity, but the changes in N_e and N_h may not be symmetric. In order to generate a Hall-coefficient sign change in this model, the initial hole and electron pockets need to have different numbers of carriers and different masses. We take $m_h=\alpha m_e$ and $N_h=\beta N_e$. With these definitions the expression for ρ_{12} in terms of $X(H)$ becomes

$$\rho_{12}=\frac{H}{N_e|e|c}\frac{\beta-X(H)+\alpha^2[X(H)-1]}{\{\beta-X(H)+\alpha[1-X(H)]\}^2} . \tag{4.8}$$

With the same definitions the magnetic resistance becomes

$$\rho_{22}=\frac{m_e}{N_e e^2\tau}\frac{\alpha}{\beta+\alpha-\alpha X(H)} . \tag{4.9}$$

Equation (4.9) has been used to fit the experimentally observed resistance versus magnetic field in order to obtain $X(H)$. The function $X(H)$ is then used in Eq. (4.8) to determine the Hall resistance ρ_{12} versus magnetic field. The data at 30 K can be reasonably well fitted using $\alpha=1.075$ and $\beta=1.105$. These values are quite reasonable for imperfect nesting where the hole and electron pockets would be comparable but with slightly different sizes and masses, depending on the nesting geometry of the FS.

The calculated values of $X(H)$, the normalized Hall resistivity and the Hall coefficient for the field range 0–160 kG are shown in Fig. 41 and the correct sign change at ~80 kG is generated. The function $X(H)$ increases from 0– ~0.6 corresponding to a major reduction of the FS pockets involved. This is comparable to the decrease in FS area required to explain the conductivity decrease observed at 227 kG if it is assigned exclusively to a FS area change induced by the improved nesting.

The actual Hall contributions may be considerably more complex than the one described by this simple model. Additional FS sheets may exist, and other contributions to the Hall mobility may be present. However, the model serves to show that the Balseiro-Falicov mechanism can easily play a role in the observed sign change as a function of magnetic field. The current dependence in the high-magnetic-field region, where CDW motion moves the zero of ρ_{12} to high fields, is certainly consistent with the Balseiro-Falicov mechanism.

3. *Magnetic-field-induced increase in the CDW transition temperature*

The Balseiro-Falicov theory[6] predicts that a high magnetic field, in the process of producing a metal-insulator transition in the relevant sheet of Fermi surface of the DW solid, may induce an increase in the DW transition temperature T_c. The value of this increase is a strong

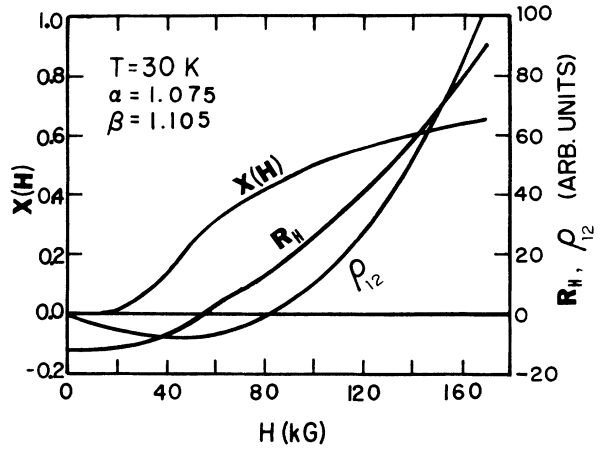

FIG. 41. The curves labeled R_H and ρ_{12} represent the calculated values of the normalized Hall coefficient and Hall resistivity using the dimensionless parameters appearing in Eq. (4.9). $X(H)$ is the magnetic-field reduction factor corresponding to the Balseiro-Falicov model and defined in Eq. (4.7). $X(H)$ is obtained by fitting Eq. (4.9) to the magnetoresistance data. An arbitrary unit scale (on the right-hand side) has been used for R_H and ρ_{12} since the model is primarily used to demonstrate the observed sign change.

function of various parameters, in particular the electron-electron interaction coupling constant and the value and orientation of the applied magnetic field. As seen in Figs. 5 and 6 of Ref. 6, the increase in T_c is large only when the coupling constant is in the vicinity of a critical value; in other ranges that increase is either very small or unnoticeable.

The data described Sec. III A 5 and shown in Fig. 17 are a tentative but clear indication that a field of 226 kG induces an increase in T_2 of approximately 0.5 K, i.e., 0.85%. This tentatively observed increase gives additional support to the Balseiro-Falicov model: it indicates that the electron-electron interaction constant, responsible for the lower-temperature CDW formation, is greater (probably less than a factor of 2) than but of the same order of magnitude of the critical value, below which the CDW state would not exist at zero value of the transverse magnetic field.

4. Temperature dependence of the threshold electric field, E_T

The observed temperature dependence of E_T in pure $NbSe_3$ crystals at $H=0$ or in magnetic fields up to 225 kG follows the thermal-fluctuation dependence given in Eq. (3.3). The experimental value of the exponent Δ/k_B was not observed to be a function of either the magnitude or direction of the magnetic field in a given crystal and values of Δ/k_B in the range $\Delta/k_B=15-20$ K were observed for different nominally pure crystals with $\mathcal{R}$'s in the range 100–250. In addition, as pointed out in Sec. III B 5, doping of $NbSe_3$ with Fe produced a major departure from the thermal-fluctuation dependence predicted by Eq. (3.3).

Maki[18] has derived the observed temperature dependence of E_T by considering the thermal fluctuation of the phase of the CDW order parameter. He has incorporated the thermal average of the phase into the Fukuyama-Lee-Rice Hamiltonian which describes the equilibrium phase configuration. This is adsorbed into a temperature-dependent threshold electric field

$$E_T(T)=E_T(0)e^{-\langle\phi^2\rangle/2}, \tag{4.10}$$

where $\langle\phi^2\rangle$ is the thermal average of the phase $\phi(x)$. Using the fact that only short-range fluctuations are important, the thermal average is calculated in terms of an anisotropy coefficient $\eta=v_1v_2/v_F$ (v_F=Fermi velocity), a stiffness constant $K=\frac{1}{6}N_0\eta v_F^2$ (N_0=density of states at the Fermi level) and a coherence length ξ. The resulting expression for $E_T(T)$ is

$$E_T(T)/E_T(0)=e^{-T/T_0}, \tag{4.11}$$

where $T_0=(2\pi)^2\eta K\xi$. Maki[18] estimates $T_0\sim 20-100$ K. Our experimentally measured values for the purest crystals are at the lower end of this range. The experimental fits of the type shown in Figs. 23–25 give values of $\Delta/k_B=T_0\simeq 15-20$ K.

V. CONCLUSIONS

The experiments and analysis reported in this paper demonstrate that the electronic properties of $NbSe_3$ arise from a complex relationship between the condensed CDW electrons and the normal electrons comprising the low-temperature FS in $NbSe_3$. This relationship plays a crucial role in both the static pinned CDW state and in the dynamic CDW motion state. In addition, both the normal FS and the CDW condensate show intrinsic modifications induced by a strong transverse magnetic field. The specific details supporting these conclusions are summarized further.

We have shown that the magnetoquantum oscillations observed in the range 1.1–4.2 K are extremely sensitive to the detailed configuration of the pinned CDW. Frequency shifts, beat structures and major changes in amplitude are observed as various metastable states of the CDW are produced in both the nominally pure and doped $NbSe_3$ crystals. The observed modifications can be uniquely generated by a model incorporating MB interference between small closed orbits and a one-dimensional open-orbit network generated by the nested FS sheets forming the CDW phase. The breakdown occurs across the CDW gap Δ, which is locally modified by the pinning configuration of the CDW. This results in a local transfer of electrons between the normal FS and the CDW condensate and produces a distribution of FS cross-sectional areas within the crystal. The MB interference remains coherent, but is a sensitive function of the precise FS area distribution being measured with a given pair of leads. This FS distribution will of course reflect any spatially inhomogeneous pinning of the CDW. Different MB interference patterns would be generated by different sections of the crystal having different pinning configurations or pinning strengths. The changes induced by depinning and repinning the CDW would also be expected to exhibit spatial inhomogeneity. We have

carried out such experiments and a range of spatially inhomogeneous effects have been observed including differences in the surface and volume pinning of the CDW. The data and analysis on these experiments are planned to be reported in a separate paper.

We have modified a previous one-dimensional open-orbit network model developed by Sowa and Falicov[10] in order to allow calculation of the magnetoresistance in two directions. The adjustable parameters are the frequency of oscillation, the frequency-distribution spread ΔF, and the critical MB field parameter $\omega_0\tau$. A fit to the experimental data generates a distribution of frequencies (FS cross-sectional areas) unique to a particular pinned CDW configuration. This distribution can be changed by depinning and repinning the CDW, heating and recooling the crystal through T_c or reversing the sign of $(\mathbf{H}\times\mathbf{I})$. Simultaneous measurement of different pairs of magnetoresistance or Hall leads gives a picture of the spatial variation in FS areas for a given pinned CDW configuration.

The quantum oscillations in doped Ni_xNbSe_3, Co_xNbSe_3, and Fe_xNbSe_3 crystals have also been studied and show a more complex pattern of oscillations than observed in the nominally pure crystals. However, the MB interference model generates good fits to the data and unique, although more complex FS cross-sectional areas are required.

The transverse magnetic field also modifies the dc background magnetoresistance caused by magnetic-field-induced mixing of the electronic bands. This can occur through a number of effects that modify the energy spectrum at the Fermi level and are important when the cyclotron energy $\hbar\omega_c$ is of the same order of magnitude as the CDW gap parameter Δ. We have observed this effect most directly at higher temperatures, where the effects proportional to $\omega_c\tau$ no longer dominate. Experiments in magnetic fields up to 220 kG have shown very large enhancement of the magnetoresistance in the temperature range 10–59 K. This strong resistance enhancement by the magnetic field is observed for all field directions lying in the **a**-**c** plane and shows an anisotropy in this plane of a factor of ~ 2, but the effect decreases to zero for **H** parallel to the **b** axis. These observations can be explained in terms of a mechanism proposed by Balseiro and Falicov[6] in which the field-induced modifications of the electronic energy spectrum drive the FS into a more perfect nesting condition and reduce the area of the remaining FS. We have summarized the theory and have shown that the experimental results are all consistent with its main points. We have also shown that the observed sign change in the Hall effect as function of magnetic field can be reasonably modeled within the framework of such a theory. A small but tentative increase in T_2 with magnetic fields has been measured, also in agreement with the Balseiro-Falicov model.

In addition to the unusual electronic effects induced by the presence of the static CDW as summarized earlier, we have also presented observations on dynamic CDW transport effects that can be readily observed in the presence of a large transverse magnetic field. At liquid-helium temperatures the I versus V behavior in a high magnetic field can show the onset of a region of zero dynamic resistance above the threshold voltage for CDW motion. This occurs at a higher threshold voltage that would be estimated from the thermal fluctuation behavior observed at higher temperatures, where we have shown that E_T follows the functional form of $E_T(T)=E_T(0)\exp(-k_BT/\Delta)$, a form also derived by Maki[18] from a thermal-fluctuation theory of the CDW. This may be evidence of the role of thermally activated normal electrons in the relaxation of the CDW in the nonlinear mode, but further experiments are needed in this area.

We have studied the effects of magnetic fields on the threshold electric field required for CDW motion in the temperature range 1.1–59 K and little evidence of an intrinsic magnetic-field induced change is observed. For the high-purity specimens E_T follows the thermal-fluctuation form and the characteristic exponent $(-k_BT/\Delta)$ shows little or no dependence on the magnitude or orientation of the magnetic field. For doped $NbSe_3$ crystals or for very low temperature, departures from the thermal-fluctuation behavior can be observed. One case of the zero-dynamic-resistance region was mentioned earlier, and in the case of Fe_xNbSe_3 there is a complete departure from thermal fluctuation behavior below ~ 25 K. Our general conclusion is that any observed magnetic-field effects on E_T are related to specific impurity pinning configurations and are not systematically reproducible. The nonlinear resistance observed in the pure crystals at high magnetic fields follows the Bardeen[14] tunneling model in the temperature range 10–50 K and a self-consistent fit can be obtained with a single thermal-fluctuation parameter k_B/Δ at all temperatures for a given crystal. Although very good fits to the high-magnetic-field measurements are obtained with the tunneling model, the range of electric fields are not sufficient to distinguish clearly from possible semiclassical models.

The quantum oscillations also show a behavior in the CDW motion regime that can be described within the framework of the tunneling model. In this case the oscillation amplitude saturates above threshold, while the background dc magnetoresistance exhibits the usual nonlinear decrease with current. A very good fit to the data can be obtained with the tunneling model, but the constant coupling the oscillating term with the nonlinear term is large indicating major magnetic-field-induced effects. These require a strong mixing of the normal quasiparticle and CDW components of the current and voltage. This may connect directly to the MB mechanism of the oscillations, which involve both the normal FS and the nested sheets. However, the nonlinear conductivity tensor needed for such an analysis has not been determined.

The Hall resistance has also been measured in both the static and dynamic CDW regime over the same temperature ranges as used for the magnetoresistance. The quantum oscillations connected with MB appear in the Hall resistance and reflect the same general relation to the FS cross-sectional area distributions as observed for the magnetoresistance. However, the Hall oscillations arise from different CDW domains of the crystal and this is reflected

in simultaneous measurements of both components which show different frequency distributions.

In the CDW motion regime the Hall resistance is a complex function of both the electric and magnetic fields. The same mechanisms that control the magnetoresistance can be used to explain many of the features observed in the Hall effect. However, the Hall resistance is a more sensitive function of the electron-to-hole ratio, the carrier mobilities, and the crystal anisotropy. Detailed analysis of these factors will require more data.

The application of high magnetic fields to $NbSe_3$ has produced a rich variety of experimental results related to the electronic structure of the CDW phase. New and unusual mechanisms have been developed to explain some of the results, while others can be analyzed with the CDW transport theories developed for zero magnetic fields. In both cases the magnetic field provides a useful additional variable to the problem, particularly at low temperature.

ACKNOWLEDGMENTS

The research at the University of Virginia was supported by the National Science Foundation Grant No. DMR-8514827. The work at the University of California, Berkeley was supported, at the Lawrence Berkeley Laboratory, by the U.S. Department of Energy, under Contract No. DE-AC03-76-SF00098. The authors wish to thank Eric C. Sowa for providing information on the computer programs used to calculate the MB models. Useful discussions have been held with C. A. Balseiro and V. Celli. Work in magnetic fields above 70 kG was performed at the Francis Bitter National Magnet Laboratory, supported at the Massachusetts Institute of Technology by the National Science Foundation. The authors wish to thank Larry Rubin and Bruce Brandt for valuable help with the experiments at the National Magnet Laboratory.

[1]P. Monceau, N. P. Ong, A. M. Portis, A. Meerschaut, and J. Rouxel, Phys. Rev. Lett. **37**, 602 (1976).

[2]R. M. Fleming, D. E. Moncton, and D. W. McWhan, Phys. Rev. B **18**, 5560 (1978).

[3]N. Shima and H. Kamimura, *Theoretical Aspects of Band Structures of Pseudo-One-Dimensional Solids,* edited by H. Kamimura (Reidel, Boston, 1985), p. 231.

[4]R. V. Coleman, G. Eiserman, M. P. Everson, A. Johnson, and L. M. Falicov, Phys. Rev. Lett. **55**, 863 (1985).

[5]R. V. Coleman, M. P. Everson, G. Eiserman, and A. Johnson, Physica **143B**, 33 (1986).

[6]C. A. Balseiro and L. M. Falicov, Phys. Rev. Lett. **55**, 2236 (1985); Phys. Rev. B **34**, 863 (1986).

[7]M. P. Everson, G. Eiserman, A. Johnson, and R. V. Coleman, Phys. Rev. B **30**, 3582 (1984).

[8]N. P. Ong and P. Monceau, Solid State Commun. **26**, 487 (1978).

[9]M. P. Everson, A. Johnson, Hao-An Lu, R. V. Coleman, and L. M. Falicov, Phys. Rev. B **36**, 6953 (1987).

[10]E. C. Sowa and L. M. Falicov, Phys. Rev. B **32**, 755 (1985).

[11]R. M. Fleming, Phys. Rev. B **22**, 5606 (1980).

[12]J. W. Brill, N. P. Ong, J. C. Eckert, J. W. Savage, S. K. Khana, and R. B. Somoano, Phys. Rev. B **23**, 1517 (1981).

[13]P. A. Lee and T. M. Rice, Phys. Rev. B **19**, 3970 (1979).

[14]J. Bardeen, Phys. Rev. Lett. **45**, 1978 (1980); Phys. Rev. B **39**, 3528 (1989).

[15]L. Sneddon, M. C. Cross, and D. Fisher, Phys. Rev. Lett. **49**, 292 (1982); L. Sneddon, Phys. Rev. B **29**, 719 (1984); **29**, 725 (1984).

[16]R. M. Fleming, J. A. Polo, Jr., and R. V. Coleman, Phys. Rev. B **17**, 1643 (1978).

[17]P. Monceau and A. Briggs, J. Phys. C **11**, L465 (1978).

[18]K. Maki, Phys. Rev. B **33**, 2852 (1986).

[19]M. P. Everson and R. V. Coleman, Phys. Rev. B **28**, 6659 (1983).

[20]A. Fournel, J. P. Sorbier, M. Konczykowski, and P. Monceau, Phys. Rev. Lett. **57**, 2199 (1986).

[21]C. G. Slough, B. Giambattista, A. Johnson, W. W. McNairy, and R. V. Coleman, Phys. Rev. B **39**, 5496 (1989).

[22]L. P. Gor'kov and A. G. Lebed, J. Phys. (Paris) Lett. **45**, L433 (1984); J. Low Temp. Phys. **42**, 101 (1981).

[23]M. Héritier, G. Montambaux, and P. Lederer, J. Phys. (Paris) Lett. **45**, L943 (1984); Mol. Cryst. Liq. Cryst. **119**, 97 (1985); J. Phys. (Paris) Lett. **46**, L831 (1985).

[24]J. Friedel, Philos. Trans. R. Soc. London, Ser. A **314**, 189 (1985).

[25]P. Parilla, M. F. Hundley, and A. Zettl, Phys. Rev. Lett. **57**, 619 (1986); M. F. Hundley, P. Parilla, and A. Zettl, Phys. Rev. B **34**, 5970 (1986).

[26]T. M. Tritt, D. J. Gillespie, A. C. Ehrlich, and G. X. Tessema, Phys. Rev. Lett. **61**, 1776 (1988).

[27]H. Fukuyama, J. Phys. Society Japan **41**, 513 (1976); H. Fukuyama and P. A. Lee, Phys. Rev. B **17**, 535 (1978).